2019

The Influence of Deep Convection on Biologically Driven Carbon Sequestration in the Irminger Sea

Lucy Wanzer
lwanzer@wellesley.edu

The Influence of Deep Convection on Biologically Driven Carbon Sequestration in the Irminger Sea

Lucy A. Wanzer

April 25, 2019

Submitted in Partial Fulfillment of the Prerequisite for Honors in Geosciences under the advisement of Hilary I. Palevsky, Ph.D.

Acknowledgements

Firstly, the biggest thank you to my thesis advisor Hilary. I have the utmost gratitude towards you. You have significantly altered my scientific journey and I will always feel so lucky to have you as an advisor. Thank you for saying yes when I asked to work with you at WHOI, even though you didn't know me and I knew nothing about oceanography. Thank you for teaching me MATLAB and helping me fix ALL the bugs. Thank you for taking me on as a summer research student and introducing me to the oceanographic community. Thank you for the 395 emails that we have sent each other over the past year and a half. Thank you for all your support, kind words, and traveling anecdotes while I applied for the Watson Fellowship. Thank you for taking me on as a TA for your class, and giving me the opportunity to grow as both a researcher and a teacher. Every week I look forward to meeting with you because you are such a compassionate, thoughtful, and inspiring human being.

A huge thank you to Dan Brabander. I would not be here, completing a senior thesis, thinking about graduate school in geosciences, and still so excited about learning science, if it weren't for you. Thank you for graciously welcoming me into your lab sophomore year. You have taught me to think deeply and critically about science from every angle: how it's conducted, who's involved, and what it means. Your infectious passion for geoscience is overwhelming, and you have taught me the value of embracing interdisciplinary perspectives. You are an incredible teacher, and I strive to emulate your ability to convey information in a way that is both thoughtful and engaging.

Thank you to all the students and faculty who have supported me in the Geosciences Department over the past four years. In particular, to Dave Hawkins, with whom I took my first four Geoscience courses, and who instilled in me a love for field work and rocks. An enormous thank you to all the students, past and present, in DJB lab. From sophomore year to senior year, DJB lab has been my home and where I've grown as a person and a scientist. Studying Paramecium Pond I learned so much – from how to run scientific instruments, to stakeholder analysis, to mass balance, to working collaboratively with other students. In particular, thank you to Sarah ST and Kim who have been my research buds and amazing friends. Sarah ST – thank you for always being my adventure buddy. I know we will have many more adventures together. Emma XJ – thank you for always being there for me, for editing this thesis, for going on a boat with me for three weeks, for letting me hug you, and for always answering my MATLAB questions. Nhia – thank you for your constant friendship and for our always existential conversations. To my other Geos seniors – Nolen, Jaws, Lauren, Sarah Wong, Shannon – you are such amazing people and I've felt so lucky to share our time at Wellesley together.

A thank you to all my other wonderful friends. You all are what makes Wellesley special to me. To Sam, Jackie, Bridget, Kate, and Rachel – I love you all so deeply. Thank you for eating

all our meals together and listening to me talk about this research for over a year now. Also to Brie, Antonia, and Angelina – thank you for always being there for me.

Thank you to my thesis committee members – Professor Rachel Stanley, Professor Erich Matthes, and Dr. David Nicholson. Thank you for agreeing to read this thesis, and for putting your time and energy into my growth as a student. Additionally, I'd like to thank the Jerome A. Schiff Fellowship for helping to support this research.

Lastly, a huge thank you to my family – to Mom, Dad, Sam, Mit, Marcy, and the entire Wanzer family. Dad – thank you for instilling in my a love of the natural world – from birding to tree identification to canoeing, you will always be my favorite naturalist. Mom – thanks for always telling the truth. I know that whenever I need advice, you will give me the honest, hilarious truth. Mit – thank you for reading all my blog posts from my time at sea, chatting with me about all things science, and always being my fiercest advocate. Marcy – thank you for being a second mom to me. You are the most joyous, wonderful, Cedar waxwing-loving woman I know, and I will always look up to you. To my grandparents, Nanna and Pop, thank you for investing so much of your time and resources into my education. I am eternally grateful.

Abstract

The North Atlantic plays a key role in sequestering anthropogenic carbon. The biological carbon pump is one of the mechanisms by which carbon is sequestered in the ocean. Phytoplankton photosynthesize at the sea surface, and fix carbon dioxide into organic carbon, a fraction of which sinks to the deep ocean. For sinking carbon to be stored long-term (time scales > 1 year), it must sink deeper than the winter ventilation depth before being respired. This study focuses on how deep winter ventilation (convective mixing to depths > 1000 m) in the Irminger Sea influences the sequestration of carbon via the biological pump. We analyze a four-year continuous time series (September 2014 to June 2018) of temperature, salinity, dissolved oxygen, optical backscatter, and chlorophyll fluorescence depth profiles from 200 to 2,600 meters from the Apex Profiler Mooring at the Ocean Observatories Initiative (OOI) Global Irminger Sea Array (60.0°N, 39.5°W). Temperature, salinity, and dissolved oxygen data are used to identify the depth and timing of winter mixing. Using dissolved oxygen as a tracer for respiration of sinking organic matter, optical backscatter as a tracer of particulate organic matter, and chlorophyll as an indicator of surface-derived photosynthetic material, the amount of sinking organic carbon ventilated back to the atmosphere in winter, as well as the carbon that escapes below the winter ventilation depth, is evaluated.

We present data collected during a research cruise to the Irminger Sea in June 2018, where we collected discrete samples to calibrate sensors on the OOI Apex Profiler Mooring, and determined variability in the depth of winter mixing across the Irminger basin (59.6˚ – 64.2˚ N and 21.9˚ – 41.4˚ W) using 20 depth profiles of temperature, salinity, and dissolved oxygen from CTD casts. Evidence of deep winter convection was found throughout the basin, though there is variability in the maximum depth of convection, ranging from 1100 to 1500 meters. Using the 2014-2018 time series of data collected by the profiler mooring, we found strong interannual variability in both winter ventilation depths and respiration rates from the in the Irminger Sea, with winter ventilation depths ranging from 800 to 1,150 meters over the four year time period, and depth-integrated respiration rates within the seasonally-ventilated thermocline ranging from 3.62 to 7.66 mol O_2 m^{-2}. We find the highest respiration rates in the upper thermocline which contribute the majority of the carbon that is released back into the atmosphere during mixing. We also find that winter ventilation depth influences how much carbon is ventilated into the atmosphere during winter mixing. This study shows the importance of year-round observations in order to better understand how deep convection influences carbon sequestration by the biological pump.

Table of Contents

Chapter 1. Introduction

1.1 Background on climate change and the ocean's role

The nineteenth century saw the extraction and burning of coal and oil at unprecedented rates, all in the name of the Industrial Revolution. As fossil fuels were extracted from the ground and combusted, carbon dioxide was released to the atmosphere. This excess carbon dioxide in the atmosphere traps heat, increasing global temperatures and changing our climate. Present day, atmospheric carbon dioxide levels have reached 414 ppm and we predict this number will continue to rise in the coming decades ("The Keeling Curve," 2019). Not all anthropogenic carbon stays in the atmosphere, a portion is taken up by both land and ocean sinks. From 1959-2017, 45% of emissions were stored in the atmosphere, and 30% in land. The ocean is also an important sink for carbon dioxide, absorbing 2.5 ± 0.5 GtC/yr, or 24%, of anthropogenic carbon in 2017 (Le Quéré et al., 2018).

Carbon dioxide is sequestered, stored long-term, in two ways: through physical circulation and through biological processes. The physical process is known as the abiotic solubility pump. As the ocean continuously exchanges gases with the atmosphere and as partial pressure of CO_2 increases in the atmosphere, CO_2 will diffuse into the ocean until the atmosphere and ocean are in equilibrium. In high latitude regions, seasonal cold temperatures and high winds create a density difference between surface and subsurface water, driving the process of deep water formation (Våge et al., 2008; Wolf et al., 2018). Gases are more soluble in colder water, so during the winter months, increased solubility drives greater uptake of CO_2 from the atmosphere. Surface water that absorbed carbon from the atmosphere sinks to depth during deep water formation, sequestering carbon for months to centuries (Sabine and Tanhua, 2010). The other key way the ocean sequesters carbon is through the biological carbon pump. Organisms at the sea surface transform carbon dioxide into organic carbon, and a portion of these organisms sink to the seafloor, storing carbon long term (Sanders et al., 2014). These processes will be described further in section 1.2.

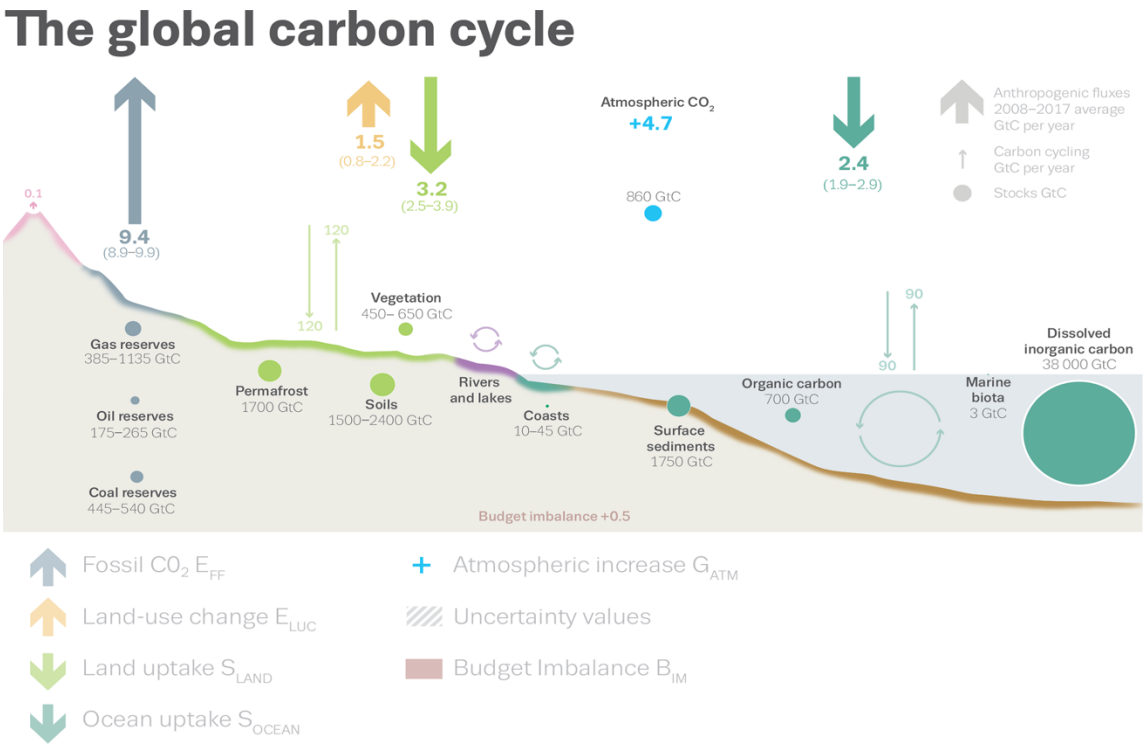

Figure 1. Diagram illustrating the impact of anthropogenic carbon in the global carbon cycle. Data is averaged globally from 2008-2017. This diagram solely illustrates the addition of anthropogenic carbon sources, which occur in addition to natural carbon cycling. Figure from Le Quéré et al., 2018.

1.2 Background on the Biological Carbon Pump (BCP)

The biological process by which carbon is sequestered in the deep ocean is known as the biological carbon pump. Phytoplankton make up the majority of the ocean's biomass, and these organisms transform carbon dioxide into organic carbon at the sea surface. After the phytoplankton die they sink through the water column where a portion are respired (converted from organic to inorganic carbon) by heterotrophic organisms. A smaller portion of the dead phytoplankton sink to the ocean floor, sequestering carbon for hundreds to thousands of years (Sanders et al., 2014).

The phytoplankton bloom occurs at the beginning of the springtime productive season when temperatures rise, and nutrients become entrained in the euphotic zone. Phytoplankton use light and nutrients to grow at the sea surface, reproducing rapidly. This event is known as the phytoplankton "bloom." Subsequently, phytoplankton are either consumed in the water column or sink to depth (Briggs et al., 2011). Of the organic material produced at the surface, typically 10-30% of organic matter sinks 100 meters below the sea surface (Sanders et al.,

2014). A substantial portion of sunken organic material is converted into inorganic carbon in the thermocline through the process of remineralization. Remineralization occurs through the consumption and respiration of phytoplankton by heterotrophic organisms. Generally, the faster phytoplankton sink, the farther they will fall in the water column. In the end, only a small fraction of the phytoplankton will fall to the seafloor and sequester carbon. The consumption of phytoplankton by zooplankton results in the production of fecal pellets (organic carbon), a portion of which are respired by bacteria as they sink or they fall to the seafloor, sequestering additional carbon (Ducklow et al., 2001).

During the springtime bloom, phytoplankton create chains and aggregate together. The formation of aggregates at the surface depends heavily on the stickiness and concentration of the particles (Briggs et al., 2011). Stickiness and concentration vary spatially and temporally, particularly because aggregation events are episodic. These factors also affect the sinking rate of the organic particles, along with other factors like size, shape, and density. For a particle to sink, it must be sufficiently large, and denser than the surrounding fluid.

1.3 The BCP in the Irminger Sea

Diatoms, single-celled autotrophs, comprise the majority of phytoplankton mass during the spring bloom (Sanders et al., 2014). The Irminger Sea has an exceptionally large springtime phytoplankton bloom compared with other regions. However, there is some debate concerning why this is the case. The magnitude of the chlorophyll peak during springtime is much higher in the North Atlantic than in other regions, such as the North Pacific. However, chlorophyll levels do not always accurately correlate with phytoplankton biomass. In the North Pacific, increases in phytoplankton biomass occurs at the same time as nutrient and light driven decreases in cellular pigment levels (chlorophyll). Therefore, in this region, increases in phytoplankton biomass are not directly correlated with increases in chlorophyll levels (Westberry et al., 2016). Conditions necessary for a phytoplankton bloom were first hypothesized by Sverdrop (1953) based on observations in the North Atlantic Ocean. Sverdrup originally hypothesized that a springtime bloom occurs when deep winter mixing shoals to a critical depth where phytoplankton growth exceeds loss (Sverdrup, 1953). More recently, Behrenfeld (2010) has contended this idea by observing that the onset of the phytoplankton bloom occurs during the

deep mixing season, in the absence of stratification. Using remote satellite data of chlorophyll concentrations, he argued that the initiation of the phytoplankton bloom begins when mixed layer depths are at their maximum during the winter, not during springtime (Behrenfeld, 2010). Although the mechanisms that produce a large bloom are not yet well understood, the Irminger Sea hosts one of the largest phytoplankton blooms which drives significant carbon export to depth.

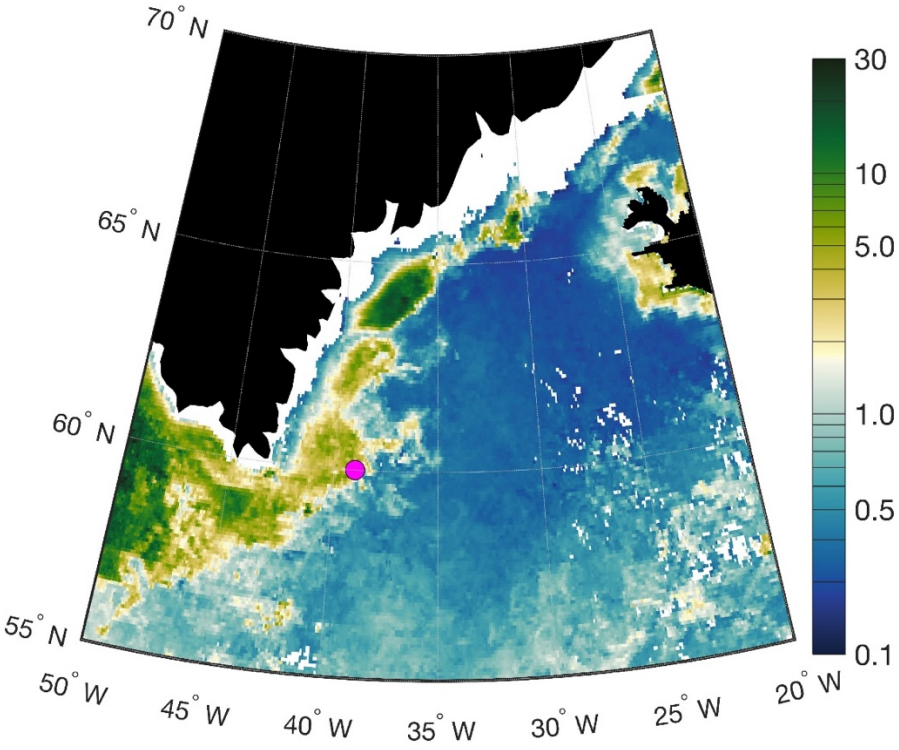

Figure 2. Sea surface chlorophyll-a (µg L^{-1}) in the Irminger Sea. Data taken from MODIS Aqua in May 2015 (Palevsky & Nicholson, 2018). Pink dot indicates location of the Irminger Sea Global Array.

The timing of the phytoplankton bloom in the Irminger Sea varies decadally and shows a correlation with atmospheric forcings, like the North Atlantic Oscillation Index (NAO) (Henson et al., 2009; de Jong & de Steur, 2016). The NAO is a climatological phenomenon that affects atmospheric pressure across the North Atlantic and occurs on decadal timescales. It is based on the difference in sea surface pressure between the Subtropical Azores and the Subpolar Atlantic (Lamb & Peppler, 1987). A positive NAO results in strong westerly winds and colder temperatures across the Irminger Sea. Colder temperatures and high winds remove more sea

surface heat, creating a strong density difference between the surface layer and the subsurface ocean. The greater difference in density leads to deeper mixed layers, delaying stratification of the water column, and delaying the start of the springtime bloom by 2-3 weeks. This idea is consistent with Sverdrup's hypothesis that for the bloom to begin, the water column must stratify so that sunlight can penetrate the water column and create the conditions necessary for phytoplankton growth (Henson et al., 2009; Sverdrup, 1953).

1.4 Deep Convection in Irminger Sea

Ocean convection is a process that occurs globally with significant spatial and temporal variation. Convection begins when the surface layer of the ocean becomes denser than the water below, resulting in the exchange of mass and heat throughout the water column. A number of high latitude regions have been identified as having particularly deep winter convection, such as the Labrador Sea, the Norwegian Sea, the Greenland Sea, the Southern Ocean, and the Irminger Sea (M. Femke De Jong et al., 2012; Wolf et al., 2018).

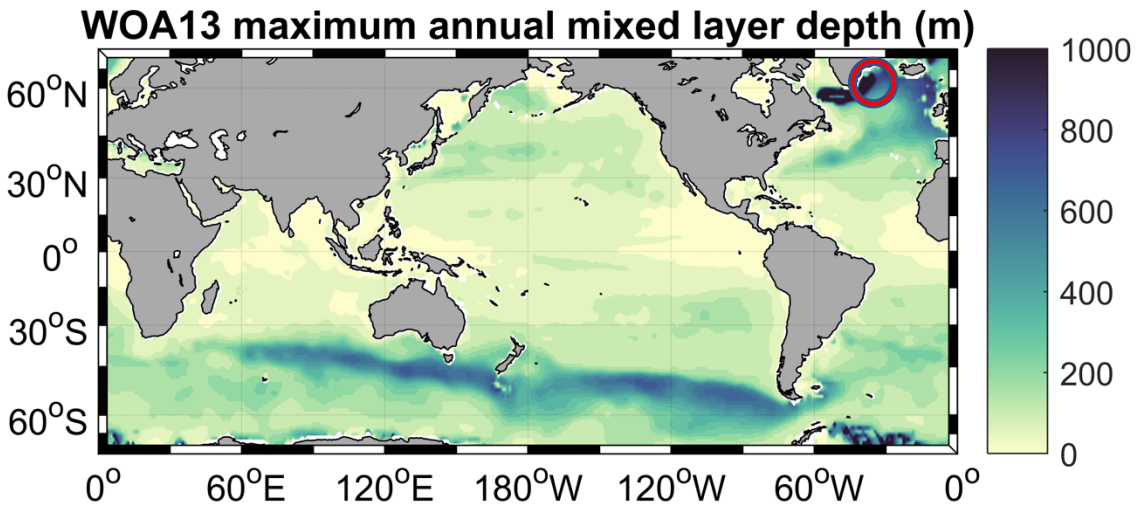

Figure 3. Global map illustrating maximum mixed layer depth. The red circle indicates Irminger Sea. Note that mixed layer depths reached <1,000 meters in this region.

Ocean convection is primarily driven by buoyancy loss, the process of surface water becoming denser due to increased salinity or colder temperatures (Marshall & Schott, 1999). Understanding the process of deep convection in the Irminger Sea is important for many

reasons, one of them being that deep convection is a key process in the Atlantic Meridional Overturning Circulation (AMOC). The AMOC is a branch of the global ocean circulation and is characterized by an upper layer of warm, northward flowing water, and a lower layer of cold, dense, southward flowing water (Lozier, 2011). The AMOC plays a key role in the ocean's ability to sequester carbon and heat from the atmosphere, and thus is a key control on climate change. Changes in paleoclimate can partially be attributed to changes in the AMOC. It is hypothesized that a decrease in the strength of the AMOC or a shutdown of the AMOC would lead to a colder arctic, and greater ice cover. A stronger AMOC is associated with a warmer arctic and less ice (Buckley and Marshall, 2015). The Irminger Sea is one of the regions where warm surface water undergoes buoyancy loss, sinks, and returns southward, forming what is referred to as an "intermediate" water mass, comprising one of the AMOC branches (Lozier et al., 2019). Previous studies focused on the Labrador Sea as the main region where deep water formation occurs, however a recent study has found that the Irminger and Iceland basins are largely responsible for driving deep water formation. Lozier et al. (2019) found that overturning in the Irminger and Icelandic basins (15.6 ± 0.8 Sv) is seven times greater than overturning in the Labrador region (2.1± 0.3 Sv).

The Irminger Sea has particularly deep convection compared with other regions (Fröb et al., 2016). This is mainly due to two factors that control open ocean deep convection: preconditioning and strong surface buoyancy forcing. Preconditioning describes the conditions of the water column prior to winter mixing, and in the case of the Irminger Sea, there is weak initial stratification prior to winter mixing. Weak initial stratification occurs when the density difference between distinct layers is weak, meaning that when convection begins there is a smaller density difference to overcome for mixing to occur. The other aspect controlling deep convection is surface buoyancy forcing, such as the NAO and the Greenland tip jet. A positive NAO year is associated with colder temperatures, stronger winds, and prolonged surface cooling, all leading to deeper mixed layers (de Jong et al., 2018). Greenland tip jet events are intermittent wind storms that blow off the Greenland Ice Sheet and bring cold air and strong winds to the Irminger Sea. This leads to increased heat removal from the sea surface, and

deeper convection (Pickart et al., 2003). Both the NAO and the Greenland tip jet are key controls on mixed layer depth in the Irminger Sea.

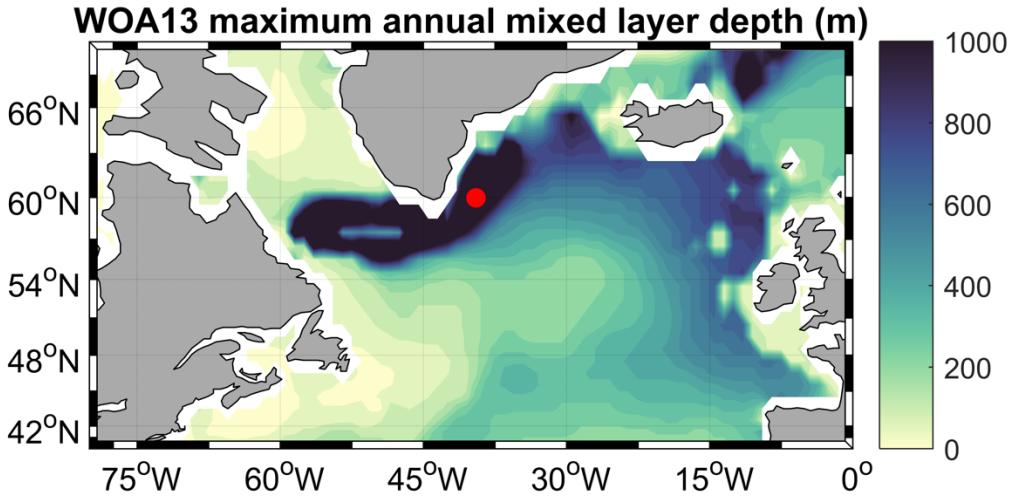

Figure 4. Maximum annual mixed layer depth in the North Atlantic Ocean. Red dot indicates study site for this research question.

Many studies have investigated the interannual and spatial variability of deep mixing in the Irminger basin (e.g. de Jong et al., 2012, de Jong and de Steur, 2016, Pickart et al., 2003, Piron et al., 2016, Våge et al., 2008). Using a 12-year time series, de Jong and de Steur (2016) identified particularly deep convection during the 2014-15 winter. Average mixed layer depth between years 2007 and 2012 ranged from 800 to 1000 meters. However, in the winter of 2014-15 mixed layer depth was exceptionally deep: 1400 meters. de Jong and de Steur (2016) found that exceptionally deep mixing was associated with a positive NAO state, and that local forcings are more likely to be responsible for changes in mixed layer depth rather than other multi-decadal changes.

Significant spatial differences in mixed layer depth during the winters of 2014-15 and 2015-16 across the Irminger basin have also been identified. de Jong et al. (2018) found differences in mixed layer depth between two autonomous mooring arrays located 85 km apart latitudinally. Before the onset of winter mixing, weather conditions and temperature profiles in each location were practically identical. However, differences began to appear at the onset of mixing in January. Lower temperatures and deeper mixed layers were found at the mooring located

farther south. At the mooring located farther north, warming events, and restratification occurred throughout the mixing season, causing shallower mixed layers throughout the winter months (de Jong et al., 2018). This study indicates the importance of understanding spatial variability in the depth of winter convection across the Irminger basin.

1.5 Connection between the BCP and deep convection in the Irminger Sea

The North Atlantic Ocean plays a key role in the natural carbon cycle and in the absorption of anthropogenic carbon, absorbing anthropogenic carbon at 3x the global rate (Sabine et al., 2004). In the Irminger Sea, the region of the North Atlantic Ocean between Iceland and Greenland, carbon sequestration via the biological carbon pump is influenced by two competing processes: a large spring phytoplankton bloom and deep winter mixing (Palevsky & Nicholson, 2018).

The springtime bloom in the Irminger Sea produces fast sinking phytoplankton aggregates, and for these aggregates to effectively store carbon, they must sink beneath the winter ventilation depth (deepest mixing depth) (Sanders et al., 2014). If the phytoplankton are remineralized within the water column, the carbon will be ventilated back into the atmosphere during deep mixing. Therefore, the amount of carbon that is sequestered via the biological carbon pump depends, in part, on the winter ventilation depth. In theory, the shallower the winter ventilation depth, the more organic material would make it past the winter ventilation depth to be sequestered long term. Conversely, if the winter ventilation depth is deeper, winter ventilation would ventilate more of the water column, exchanging more carbon back into the atmosphere (Körtzinger et al., 2008). Additionally, the strength of the springtime bloom affects how much carbon is sequestered. A larger bloom would not only produce more phytoplankton for sequestration, but also affects the formation of aggregates, and sinking rates. A larger bloom includes the formation of larger aggregates and larger-celled phytoplankton, leading to more carbon export (Sanders et al., 2014). In this way, carbon sequestration via the biological pump can be thought of as a competing process between biological carbon export and deep convection. Ultimately, both the biological carbon pump and deep convection have significant annual variation, so when studying carbon sequestration via the biological carbon pump, the

two processes must be considered in tandem (Körtzinger et al., 2008; Palevsky & Nicholson, 2018).

Palevsky and Nicholson (2018) investigated a two-year data set (2014-16) of biogeochemical data in the Irminger Sea, looking into the effects of deep mixing on carbon sequestration. They observed a large increase in dissolved oxygen concentrations during the spring bloom, signifying high autotrophic activity. As the stratified season progressed, oxygen concentrations declined, indicating high rates of respiration and remineralization. Over the 2015 stratified season, they observed that 8.3 mol O_2 m^{-2} was consumed by respiration, which corresponds to 5.9 mol C m^{-2} ventilated back into the atmosphere the following winter, indicating a reduction in potential carbon sequestration.

Kortzinger et al. (2008) studied a two-year time series (2003-2005) of data from a site in the northeast Atlantic Ocean, consisting of data that included the partial pressure of CO_2 (pCO2), mixed layer depth, and biological measurements. Temperature changes have a strong influence on the pCO_2 cycle, so before analyzing the data, they first corrected the data by removing the thermal effects on pCO_2. They discovered a seasonal pCO_2 cycle that consisted of a summer pCO_2 minimum and a winter pCO_2 maximum. The summer minimum was attributed to the dominance of biological factors over physical factors, while during the winter months, physical factors were dominant. They found that the onset of winter ventilation reventilated more than one third of the carbon that was drawn down by biological processes, approximately 3.6 mol C m^{-2} (Körtzinger et al., 2008).

1.6 Overview of methods and research question

Using a four-year dataset, collected by a profiler mooring that is managed by the Ocean Observatories Initiative (OOI), we analyze biogeochemical and physical data in order to better understand the connections between deep convection and the biological carbon pump. OOI is an NSF funded program that deploys and manages mooring arrays around the world, and one of these mooring arrays is the Global Irminger Sea Array, situated between Iceland and Greenland. We mainly use data collected by the wire-following profiler attached to the profiler mooring: an instrument that moves up and down in the water column continuously collecting data. Prior to OOI, there were few time series datasets that included both physical and

biogeochemical collected in high latitude regions. This dataset provides a unique opportunity to investigate the connections between the biological carbon pump and deep mixing in this region.

Many prior studies have investigated the export of carbon from the surface ocean during the spring bloom, but few studies have had data to look at what happens to the carbon throughout a full annual cycle. This research will build on previous work by investigating a four-year time series (2014-2018) of data containing both biogeochemical and physical parameters, allowing us to look at the connections between the biological carbon pump and deep convection. Investigating these factors over a four-year period, we will be able to better understand how interannual variability of deep convection affects the amount of carbon that either escapes below winter ventilation depth or is re-ventilated to the atmosphere.

We use oxygen, chlorophyll, and backscatter data collected by the profiler mooring in order to investigate this research question. Using oxygen data, we identify annual mixed layer depth and calculate annual respiration rates. During the winter ventilation season, oxygen concentrations rise as the water column is vigorously mixed and exposed to the air. We identify the depth of the mixed layer based on the depth at which oxygen concentrations drastically change. Once the water column has stratified, oxygen concentrations steadily decrease overtime as respiration is dominant over photosynthesis. In order to calculate annual respiration rates, we subtract the minimum oxygen concentration at the end of the stratified season from the oxygen maximum at the end of the mixing season. We also employ a second method of calculating respiration rates using a linear fit model to find a rate of change per day at each depth in the water column. Both methods involve integrating over the entire water column for each stratified season in order to calculate annual respiration rates. We also perform preliminary attempts at calibrating the backscatter dataset using discrete particulate organic carbon measurements taken during the most recent mooring deployment cruise. Using the chlorophyll time series, we identify how chlorophyll can be used as a tracer for deep mixing, and with further calibration will allow us to quantify the amount of organic material that sinks below the winter ventilation depth.

Chapter 2. Methods

2.1 Background on the Ocean Observatories Initiative (OOI)

The Ocean Observatories Initiative (OOI) is an NSF funded program that aims to collect long-term data sets through autonomous sensors that are deployed year round (Smith et al., 2018). OOI manages six mooring arrays throughout the Atlantic and Pacific Oceans. Two of the mooring arrays are located coastally, and the four others are situated in the open ocean. One of the global mooring arrays is located in the Irminger Sea, a region where stormy weather has limited the ability of scientists to collect data from seagoing vessels during winter months. Therefore, the only way to collect data during winter months is from autonomous sensors. Previously there have been long-term moorings in the Irminger Sea collecting physical oceanography data (de Jong et al., 2012), however OOI is the first array to have biogeochemical sensors as part of the instrument packages. By operating continuously throughout the year, the Irminger Sea Global Array collects full seasonal cycles of data, which are crucial to fully understanding the processes operating in this region. The Irminger Sea Global Array was first deployed in September 2014, and OOI plans to sustain this array for 25 years.

The Irminger Sea array hosts four moorings: a surface mooring, two subsurface moorings, and a profiler mooring. The data for this study was collected by the wire following profiler that moves along the profiler mooring. The wire following profiler is an instrument that continuously moves along a wire between 200 and 2,600 meters collecting both biogeochemical and physical data (59.9695°N, 39.4886°W). This study used dissolved oxygen, chlorophyll-a, backscatter, temperature, and salinity data collected by the profiler mooring. The wire-following profiler contains a Sea-Bird - SBE 52MP CTD that measures conductivity, temperature, and depth, a WET Labs – FLBBRTD 2-Wavelength Fluorometer that measures both chlorophyll and optical backscatter, and an Aanderaa - Optode 4330 that measures dissolved oxygen.

The OOI dataset used in this study includes data from September 2014 to August 2018 collected by the wire-following profiler. The wire-following profiler makes approximately 1 profile per day. We took the averages values of each data type from the paired up and down

profiles so as to mitigate bias from data measured in a single direction. After taking the paired up and down averages, a total of 784 profiles are included in the dataset. Biogeochemical sensor data were calibrated prior to analysis (see section 2.4 for dissolved oxygen calibration and section 2.3 for discrete sample validation of backscatter and chlorophyll-a data).

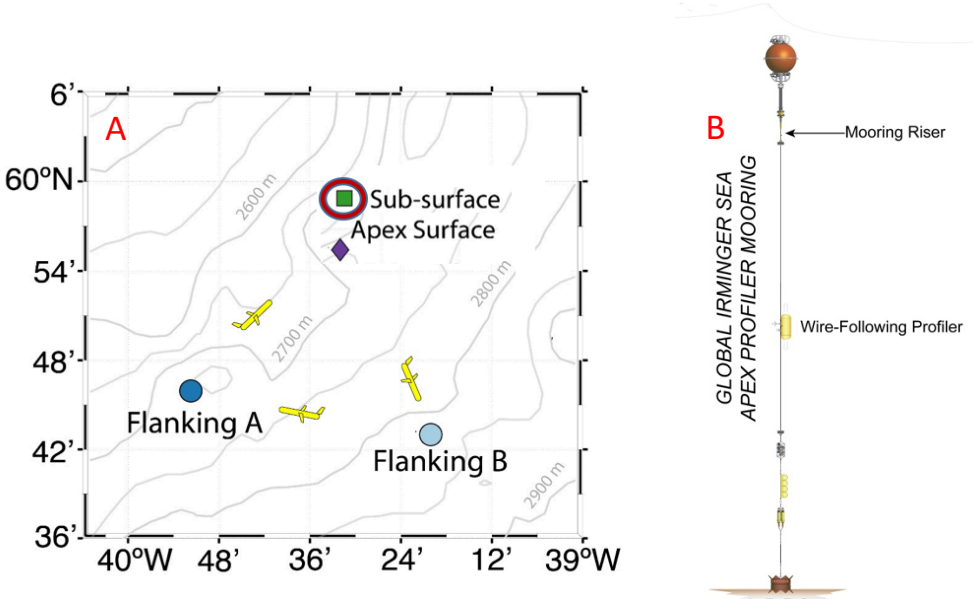

Figure 5. A) map of Irminger Sea Array showing the locations for the 4 moorings. The red circle indicates the location of the sub-surface profiler mooring. Figure from (Palevsky & Nicholson, 2018). B) Schematic of the profiler mooring, including the wire-following profiler that moves along the mooring collecting data. Figure credit to OOI.

2.2 Background on types of data used in this study

Dissolved oxygen data can be used to calculate the balance between photosynthesis and respiration, and also can be used as a tracer for ventilation. Dissolved oxygen concentrations are an indicator of how much carbon was respired in the water column, allowing us to calculate respiration rates. In a system where autotrophs are the dominate species, we expect net photosynthesis, while in a system where heterotrophs dominate, we expect net respiration (Henson et al., 2009; Sanders et al., 2014). Oxygen is stoichiometrically related to carbon in photosynthesis and respiration with a ratio of 1.4 O_2 to 1 C (Laws, 1991). This relationship allows us to calculate net production or consumption of carbon. We can also use oxygen as a tracer to identify the deepening of the mixed layer during winter ventilation. Oxygen concentrations rapidly increase as subsurface waters are ventilated, and concentrations continue to increase throughout the mixing season.

Chlorophyll-a measurements are made using a 2-Wavelength Fluorometer that measures chlorophyll-a fluorescence. During the spring bloom, chlorophyll a concentrations are high, allowing us to identify the beginning and duration of the springtime bloom. Measurements of chlorophyll-a levels throughout the water column indicate how much organic matter sinks out of the sea surface. Chlorophyll measurements can also trace the deepening of the mixed layer during winter ventilation.

Particulate organic carbon (POC) measurements were made using the 2-Wavelength Fluorometer. Backscatter is calculated by measuring the volume scattering function, and is another way to measure the amount of carbon in the water column. This data will give us another parameter to measure organic carbon concentrations in the water column and the amount of carbon that sinks below the winter ventilation depth.

Temperature and salinity measurements were made using a Seabird CTD Rosette. These are two key physical variables that control density, and therefore stratification, in the water column.

2.3 Irminger Sea cruise and spatial variability data

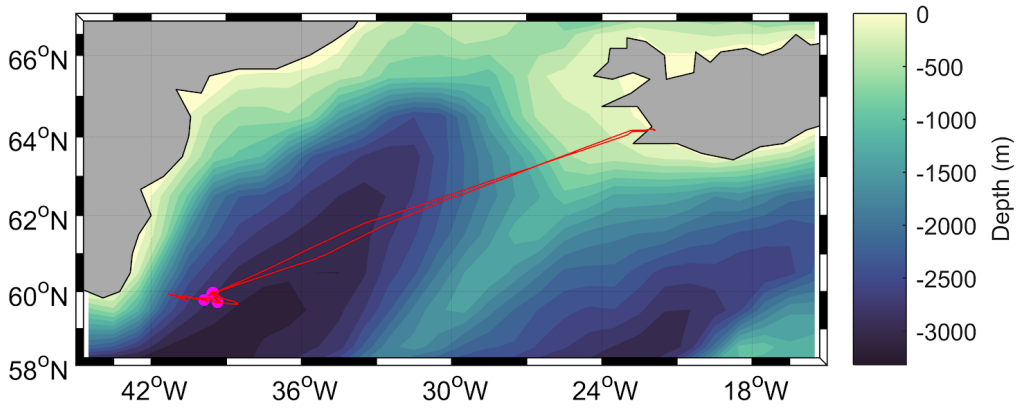

Figure 6. Cruise track overlain on bathymetric map of Irminger Sea. Pink dots indicate locations of the moorings in the Irminger Global Sea Array.

From June 5-24 2018, I participated in the Irminger-005 OOI cruise cruise aboard the R/V Neil Armstrong. We departed out of Reykjavik, Iceland, steamed to the Irminger Sea Global Mooring Array, serviced the mooring array, and returned to Reykjavik. The Wellesley group aboard the ship consisted of myself, Dr. Hilary Palevsky, and Emma Jackman (’19).

During the research cruise, 22 CTD casts were performed. A CTD cast collects discrete water samples from depth and measures physical and biogeochemical properties of the water column, including dissolved oxygen. As it is named, a CTD instrument measures conductivity, temperature, and depth. An array of bottles, called a rosette, along with the CTD, are lowered into the water column. As the rosette and CTD are raised through the water column, individual bottles close at particular depths to capture seawater. The majority of the CTD casts during the cruise were taken in order to calibrate the sensors on the mooring arrays. Our group collected discrete water samples from 9 of the CTD casts in order to calibrate the instruments in the mooring array.

We collected water samples from the sea surface and from depth to analyze dissolved oxygen, chlorophyll, and particulate organic carbon (POC) concentrations. Dissolved oxygen samples were collected by letting 2-3 volumes of water flow through the collection bottle, adding reagents, and shaking the bottle approximately 20 times. Discrete samples were measured onboard using a custom-built Winkler titrator, with automated potentiometric endpoint detection (Carpenter, 1962).

Chlorophyll samples were collected by filtering 1-2 liters of seawater through a 25mm GFF filter. Samples were then frozen onboard and later measured using a Turner fluorometer (Ashe 2004 & Laney 1998). 90% acetone was used to extract chlorophyll sample in a 10ml vial. The amount of acetone used to dilute the sample was determined based on chlorophyll levels, which could be estimated based on the greenness of the sample. Duplicates were run for each sample, and acetone blanks were run every five samples.

POC samples were collected by filtering 1-2 liters of seawater through a pre-combusted filer to remove any background organic carbon from the filter. POC measurements were made on filtered suspended solids with a CE Instruments Flash EA 1112 elemental analyzer. Using a micro-Dumas combustion technique, filters are combusted with oxygen and other reagents which reduces organic carbon and carbon dioxide to nitrogen and nitrogen oxides. Nitrogen oxides were reduced to N2 which can be detected and measured by thermal conductivity detectors (Ehrhardt and Koeve, 2007).

Table 1. Samples collected on the Irminger-005 cruise during June 2018.

Sample Type	CTD discrete samples
Dissolved Oxygen	224
Chlorophyll	37
Particulate Organic Carbon (POC)	25

In order to understand how deep convection varied spatially during the 2017-18 mixing season, we analyzed the CTD casts that reached or surpassed 1,500 meters below the sea surface of the water column, totaling 17 of the 22 casts. Using temperature and salinity data, we calculated density, and used this a proxy for the previous year's winter ventilation depth. Additionally, apparent oxygen utilization (AOU) was used a proxy for mixed layer depth and was calculated by subtracting actual measured values of oxygen concentrations from the concentration of oxygen expected at saturation. Oxygen data from the CTD was not calibrated prior to calculated AOU. We don't expect this to interfere with our analysis, as we are looking at how oxygen changes with depth, not absolute values. Oxygen saturation was calculated from temperature and salinity based on the equation of Garcia and Gordon (1992).

(Eq. 1) $AOU = O_2 - O_2\ SAT$

2.4 Oxygen calibration

Dissolved oxygen data collected by the Aanderaa optode on the profiler mooring must be calibrated for initial pre-deployment drift and post-deployment drift in order to ensure accurate measurements. Oxygen calibration is a crucial step in the research process, allowing us to obtain the most accurate oxygen in order to make the most accurate interpretations of how much carbon is respired in the water column.

At the time of deployment for the Aanderaa optode, the optode had drifted from its initial factory calibration. In order to correct for pre-deployment drift, we compare discrete oxygen sample measurements taken from the Irminger-005 cruise and previous Irminger Sea cruises (2014-2017) with oxygen measurements taken by the profiler mooring. Discrete samples used to calibrate data from 2014 were collected during the R/V Knorr 221-04 cruise, samples used to calibrate 2015 data were from the R/V Atlantis 30-01, samples used for 2016

data were from the R/V Armstrong 07, and samples for 2017 came from the R/V Armstrong 21. Discrete samples from these cruises were collected and measured following similar methods from the Irminger-005 cruise. We compared profiles that were taken within 1 day of the CTD cast, measurements that were within 20 meters vertically of Winkler sampling depth, and profiles that were within 30 kilometers away distally. Additionally, a gain correction was only calculated if the standard deviations of the oxygen measurements from the profiler were within 5 standard deviations of the discrete oxygen measurements.

After comparing the dissolved oxygen CTD profiles that aligned with the oxygen profiles from the profiler mooring, a gain correction was calculated that accounts for the difference between Winkler-measured oxygen values and profiler-measured values. The gain correction was calculated for each year and multiplied by all oxygen values for the respective year. Uncertainty was also calculated for each cast when comparing the oxygen profile from the casts to the oxygen profile from the profiler mooring.

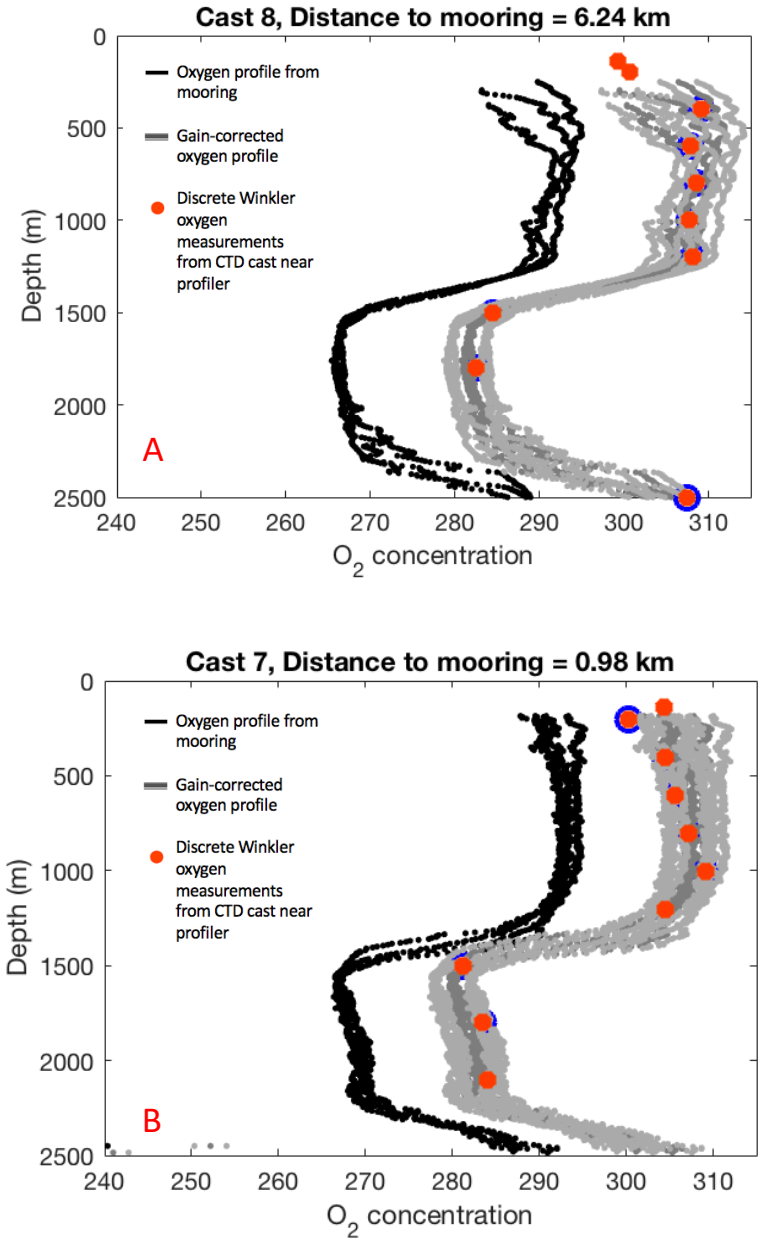

Figure 7. Examples of gain corrected oxygen profiles from 2016 (A) and 2017 (B) of deployment. Uncertainty in the gain correction is the standard deviation of the gain correction values determined across all of the profiler-Winkler measurement pairs in the aligned casts. Standard deviation is calculated and plotted for lower and higher values.

As the Aanderaa optode sits in the water column throughout the year, it changes in sensitivity overtime. In order to obtain the most accurate dissolved oxygen data, we must also correct for instrument drift over time. To correct for drift over time, we assumed that oxygen levels in the deep ocean do not change throughout the year. This method has been used

elsewhere as a proxy for instrument drift (Takeshita et al., 2013). Using this assumption, we looked at how the optode measurements changed throughout the year at 5 stable deep isotherms: 2.3, 2.5, 2.7, 2.9, and 3.1 degrees Celsius, which correlate to average depths of 2,500, 2,400, 2,300, 2,200, and 2,000 meters. Any change in dissolved oxygen levels at these isotherms would be an indication of optode drift over time, not a real signal due to physical or biological processes, in particular because we expect negligible respiration at these depths. Stable non-outlier deep isotherms were identified and a linear regression was fit to determine the slope. Using the slope, we calculated a drift rate of how oxygen levels changed over the course of a year. The standard deviation was calculated for each stable isotherm (Table 2).

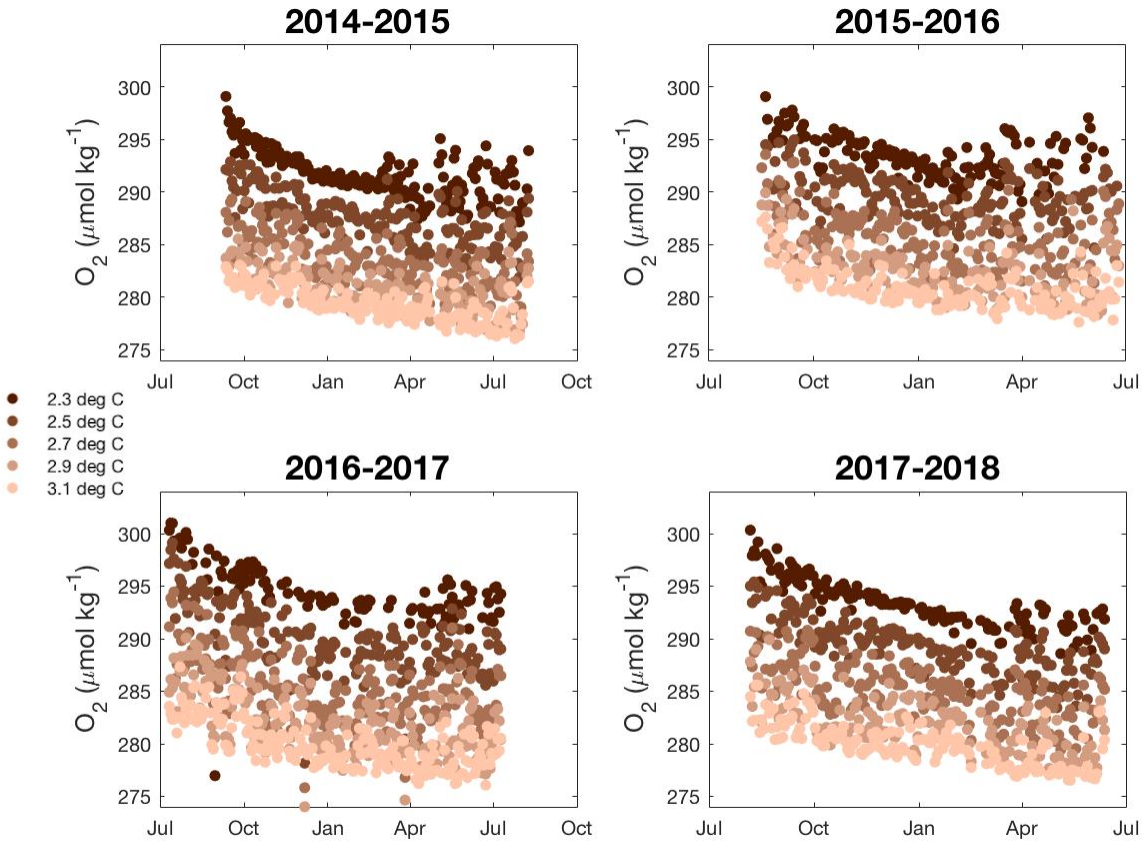

Figure 8. Post deployment drift overtime for Years 1-4 on five deep isotherms. Oxygen measurements taken by the profiler mooring. Colors indicate the 5 deep isotherms that were identified.

Table 2. Dissolved oxygen calibrations for all years.

Year	Initial Gain correction (µmol kg^{-1})	Drift over time (µmol kg^{-1}/ yr)
2014-2015	1.10 ± 0.03	-5.11 ± 0.73
2015-2016	1.13 ± 0.009	-3.29 ± 0.36
2016-2017	1.05 ± 0.008	-5.48 ± 1.095
2017-2018	1.06 ± 0.008	-6.57 ± 1.095

2.5 Winter ventilation depth calculations

Oxygen can be used as a tracer for water column ventilation. Oxygen concentrations are reset towards equilibrium with the atmosphere when the water column is ventilated, increasing concentrations in deeper layers where oxygen is undersaturated The depth in the water column where oxygen measurements dramatically shift indicates the place at which the water column was not in contact with the atmosphere. Common algorithms for mixed layer depth are often based on temperature or density change from the surface (de Jong et al., 2012; Våge et al., 2008), however we were unable to use this method due to the lack of continuous sea surface data. Instead we found winter ventilation depths by identifying where in the water column dissolved oxygen concentrations rapidly changed.

2.6 Respiration rate calculations

Dissolved oxygen values record the balance between photosynthesis and respiration, and therefore can be used to calculate respiration rates in the water column. At the end of the mixing season, oxygen concentrations reach a maximum due to input of oxygen from the atmosphere while the layer is ventilated. Once the water column stratifies and the spring bloom begins, organic matter sinks out of the sea surface. This organic matter is gradually eaten by heterotrophs as it is sinking through the water column. The heterotrophs respire the organic matter, converting organic carbon into inorganic carbon, and reducing oxygen concentrations. By the end of the stratified season, oxygen levels have reached a minimum. Therefore, in order to calculate the respiration rate for a particular stratified season, we subtract minimum oxygen values from maximum oxygen values at each depth to calculate a respiration rate. I calculated respiration rates after smoothing the data by taking the moving mean across 15 sequential depth profiles.

The timing of stratification is different at each depth in the water column, as deep isotherms tend to stratify sooner than near surface isotherms. In order to accurately capture the difference in stratification time for each depth, we identified a time range for both the onset and the end of stratification that encompasses the dates of stratification for each depth. Within this time range, we identified the maximum and minimum oxygen concentrations every 5 meters, and subtracted these values to get a respiration rate at each depth.

(Eq. 2) Stratified Season Respiration = O_2 maximum at end of winter ventilation – O_2 minimum at end of stratified season

Once we have calculated maximum and minimum oxygen values for each depth in the water column, we are able to integrate through the water column to get a total respiration rate for each year. For each stratified season, we integrated to the winter ventilation depth of the following year in order to calculate how much carbon is ventilated back into the atmosphere the following winter. The stoichiometric relationship of oxygen to carbon (O_2:C ratio of 1.4) allows us to convert respiration values from oxygen to carbon (Laws, 1991). A second method is also employed to calculate respiration rates and is discussed in section 3.3.

Chapter 3. Results and Discussion

3.1 Spatial variation in winter ventilation depth over the 2017-18 mixing season

To understand how winter ventilation depth (the deepest annual mixed layer depth) varies spatially across the Irminger Basin, we analyzed 17 apparent oxygen utilization (AOU) and density profiles to identify winter ventilation depth (Figure 9). Using AOU profiles, winter ventilation depth was determined by identifying the place in the water column where AOU concentrations dramatically increase. An increase in AOU corresponds with a decrease in dissolved oxygen concentrations, due to consumption by respiration. The mixed layer is ventilated when water is in contact with the atmosphere, enabling us to identify the winter ventilation depth as the point of sharp increase in the AOU profile.

A similar technique was employed to identify winter ventilation depth using density profiles, as the depth where density increases indicates the depth to which the water column was mixed the previous winter. Although these profiles were made in the summer, both oxygen and density can be used to determine the deepest layer that was ventilated the previous winter. After analyzing these profiles, we binned CTD profiles by shallower (1100-1200 m), average (1200-1350 m), and deeper (1350-1500 m) winter ventilation depths. To investigate the spatial relationship between winter ventilation depth and location in the Irminger basin we plotted the profiles on a map (Figure 10).

We found that winter ventilation depth varied across the Irminger Basin from 1,100 to 1,500 meters, which are among the deepest mixed layer depths found anywhere in the global ocean. Globally, mixed layer depths generally range from 25-250 meters (Kara et al., 2003). By contrast, the winter ventilation depths that we found, which exceed 1,000 meters, are exceptionally deep. In the context of the Irminger Sea, the winter ventilation depths that we found were much deeper than the average winter ventilation depth over the past 17 years. Between 2002 and 2010, winter ventilation depths in the Irminger Sea surpassed 400 meters annually, and in certain conditions reached 1,000 meters (de Jong et al., 2012). During the 2014-2015 season, de Jong and de Steur (2016) found winter ventilation depths that reached 1,500 meters. The deep mixing we observed was likely due to a combination of the strong

atmospheric forcing that de Jong and de Steur (2016) found during the 2014-15 season, as well as preconditioning following this initial year of deep mixing.

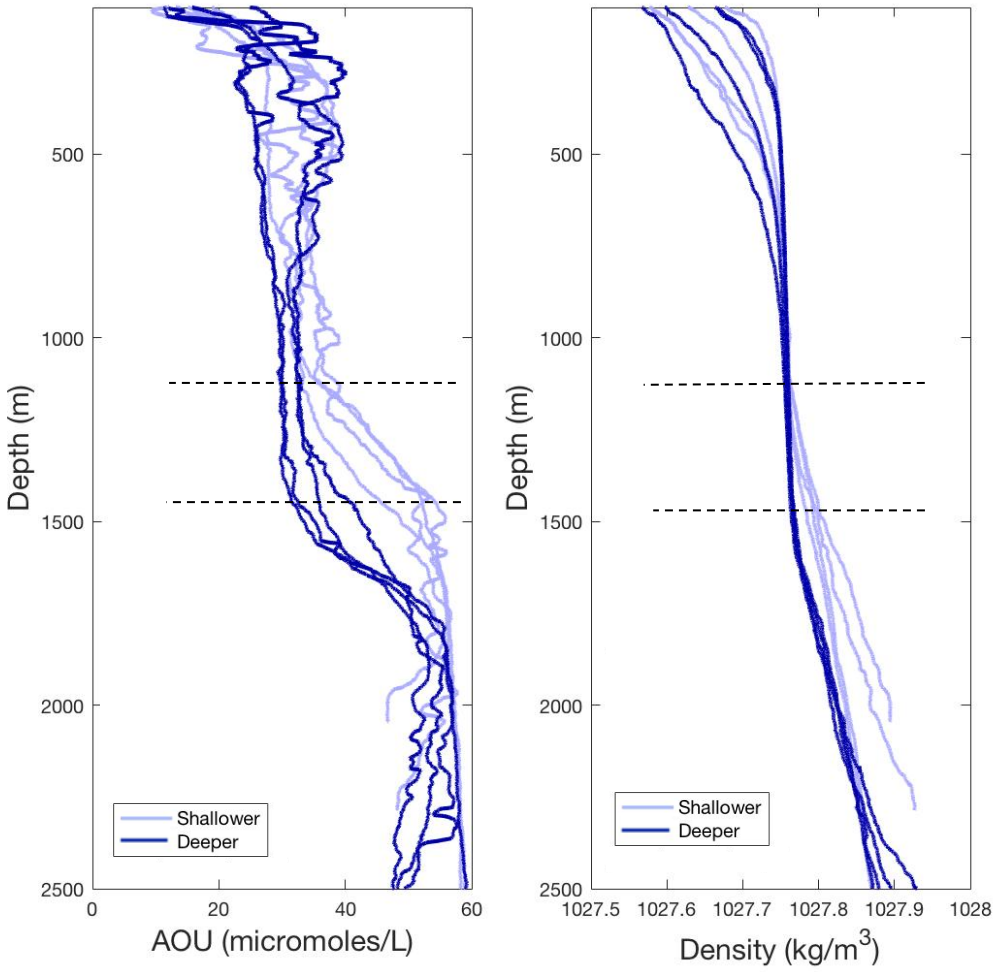

Figure 9. Depth profiles of selected casts from Irminger-005 cruise illustrating apparent oxygen utilization (AOU) and density. Light blue colored casts illustrate shallower (1100-1200 m) winter ventilation depths and purple casts illustrate deeper (1350-1500 m) winter ventilation depths. Dashed lines indicate winter ventilation depths.

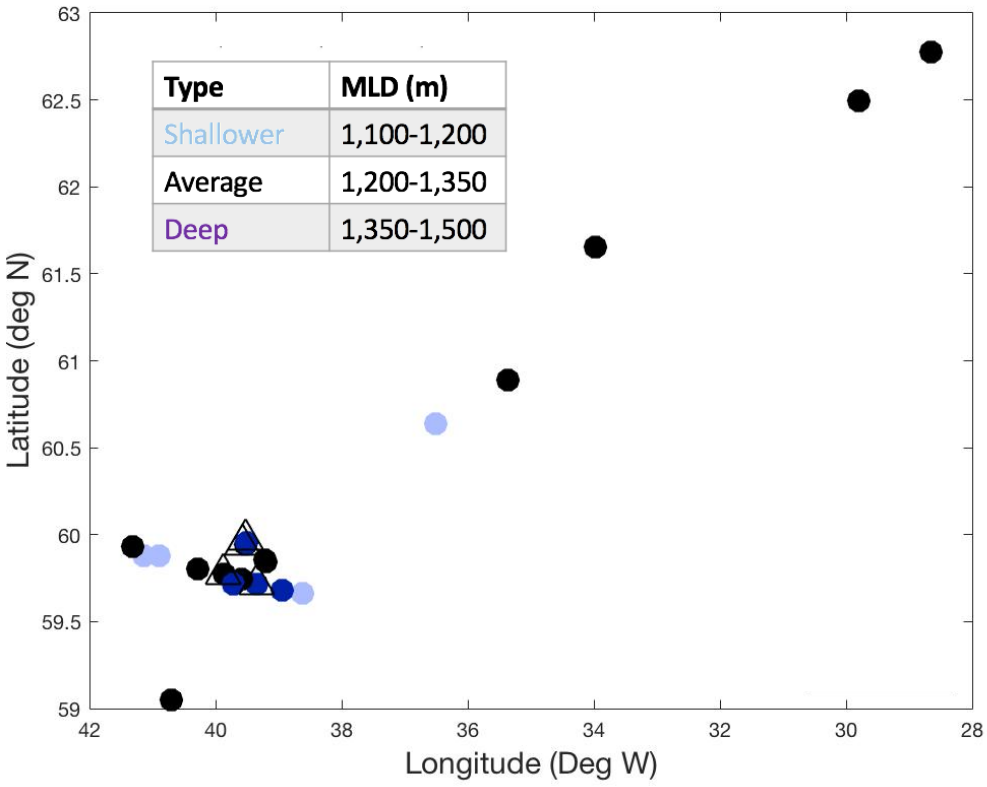

Figure 10. Map illustrating selected casts across the Irminger Basin. Casts are color coded by winter ventilation depth. Triangles indicate the locations of the OOI array moorings. Note that we did not find any clear relationship between winter ventilation depth and location within the Irminger basin.

After grouping CTD profiles by depth and plotting the profiles on a map of the Irminger basin, we did not find any clear spatial patterns between winter ventilation depth and location (Figure 10). By contrast, a regional analysis by de Jong et al. (2018) compared the profiler mooring in the Irminger Sea Global Array with two other local mooring arrays. This study found the greatest difference in mixed layer depth between the northernmost and southernmost mooring arrays, and attributed these annual differences to variation of strength in atmospheric forcings and the occurrence of intermittent re-stratification periods (de Jong et al., 2018). At most, the differences in mixed layer depth between the two mooring arrays varied by 200 meters over the 2014-15 winter season. This study is consistent with our findings in that we found variations in winter ventilation depth on the order of 100-200 meters at most. However, our findings differed in that we did not find any clear North-South pattern.

Analyzing CTD profiles across the Irminger basin allows us to better understand how deep mixing varies spatially, and the extent to which data collected from one location can represent patterns across the entire basin. In the following sections, we will be analyzing time series data taken from one location in the Irminger Sea in order to understand annual variation in winter ventilation depth across the Irminger Sea. Our analysis of the spatial patterns of winter ventilation depth across the Irminger Sea indicates that deep winter ventilation observed at the profiler mooring is representative of widespread deep mixing throughout the region, though future work will be needed to fully characterize the influence of the spatial variability in mixing throughout the region.

3.2 Variation in interannual winter ventilation depth

Using a four year time series data set, we aim to identify the annual winter ventilation depth, investigate the variability among these winter ventilation depths, and understand how these winter ventilation depths fit into the pattern of winter ventilation depths in the Irminger Sea over the past two decades. Time series oxygen concentrations taken by the profiler mooring (Fig. 11) show both deep mixing and respiration signatures for each year. In the context of our research, we define winter ventilation depth as the deepest depth at which oxygen was mixed in from the atmosphere during ventilation. We determined winter ventilation depths using a qualitative approach, looking at both the time series data and the maximum oxygen concentration depth profiles (Figs. 11-12). Over this four-year period we see some variation in winter ventilation depth, the deepest layer mixed into contact with the atmosphere each year (Figs. 11-12).

Maximum oxygen concentrations occur at the end of ventilation after the water column has been mixed for the winter season (Fig. 12). The depth in the water column where oxygen concentrations begin to rapidly decrease is the transition region from the ventilated layer to the portion of the thermocline that was not in contact with the atmosphere. Figure 12 clearly illustrates the winter ventilation depth for each year, showing a rapid decrease in maximum O_2 at 1,050 meters (~305 µmol kg^{-1}) for 2015-16, 1,150 meters (~307 µmol kg^{-1}) for 2016-17, and 800 meters (~309 µmol kg^{-1}) for 2017-18.

During the 2014-15 season, winter ventilation depths reached deeper than 1,000 meters for the first time in many years (de Jong & de Steur, 2016). This increased the oxygen concentration as the mixed layer deepened, with atmospheric oxygen penetrating into waters that had previously been isolated from contact with the atmosphere. After this year of exceptionally deep ventilation in 2014-15, evidence of this recent ventilation is seen in slightly higher oxygen concentrations (~290-300 µmol kg^{-1}) at depths reaching 1,300 meters.

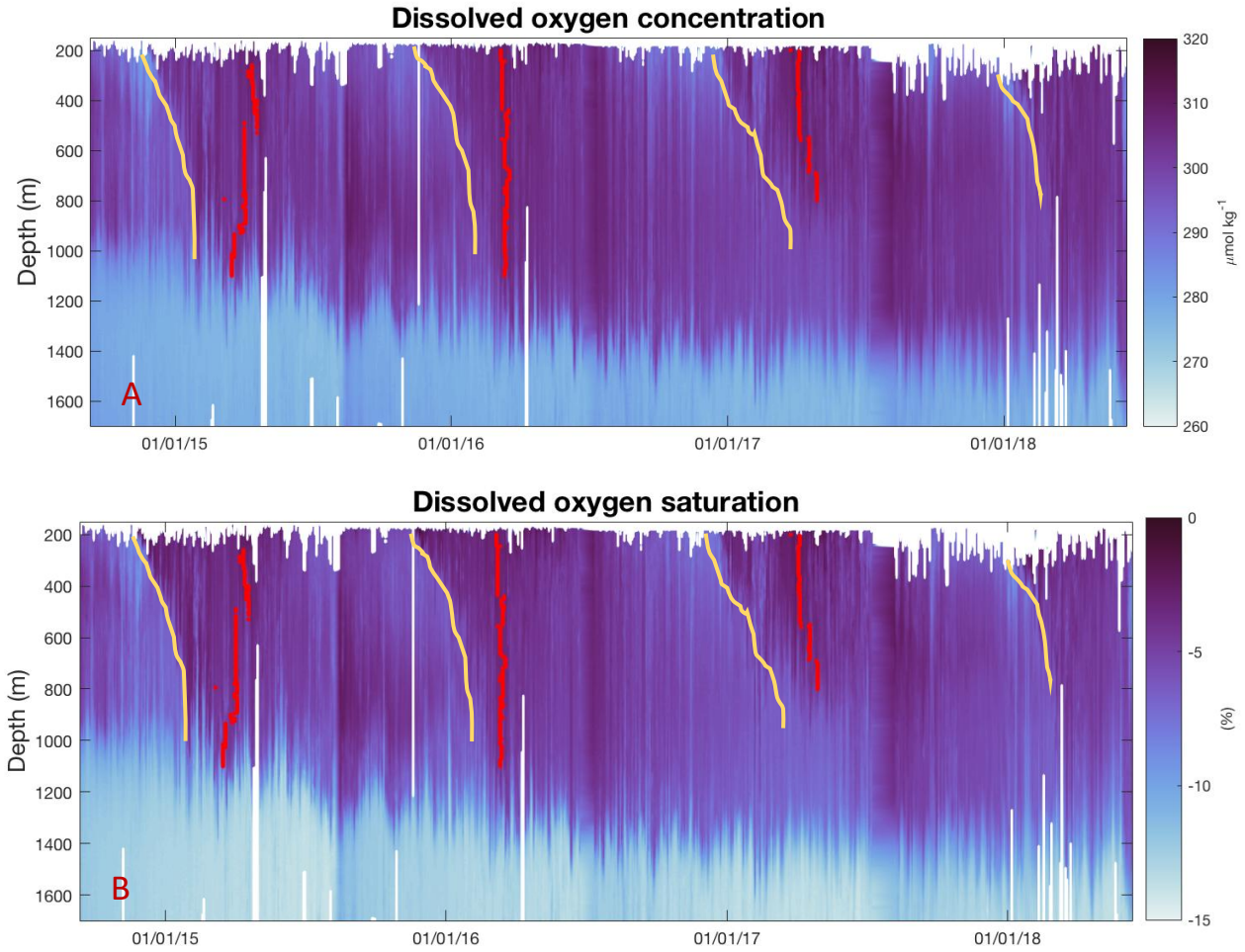

Figure 11. Time series of A) Dissolved oxygen concentration and B) Dissolved oxygen saturation for the four-year time period. Yellow lines indicate the beginning of winter ventilation, and red lines indicate the end of the winter ventilation and the onset of stratification. Yellow lines are a qualitative estimation of the onset of ventilation based on changes in dissolved oxygen concentrations. The end of winter ventilation was determined by identifying the maximum oxygen concentration at each depth, and are indicated with red lines.

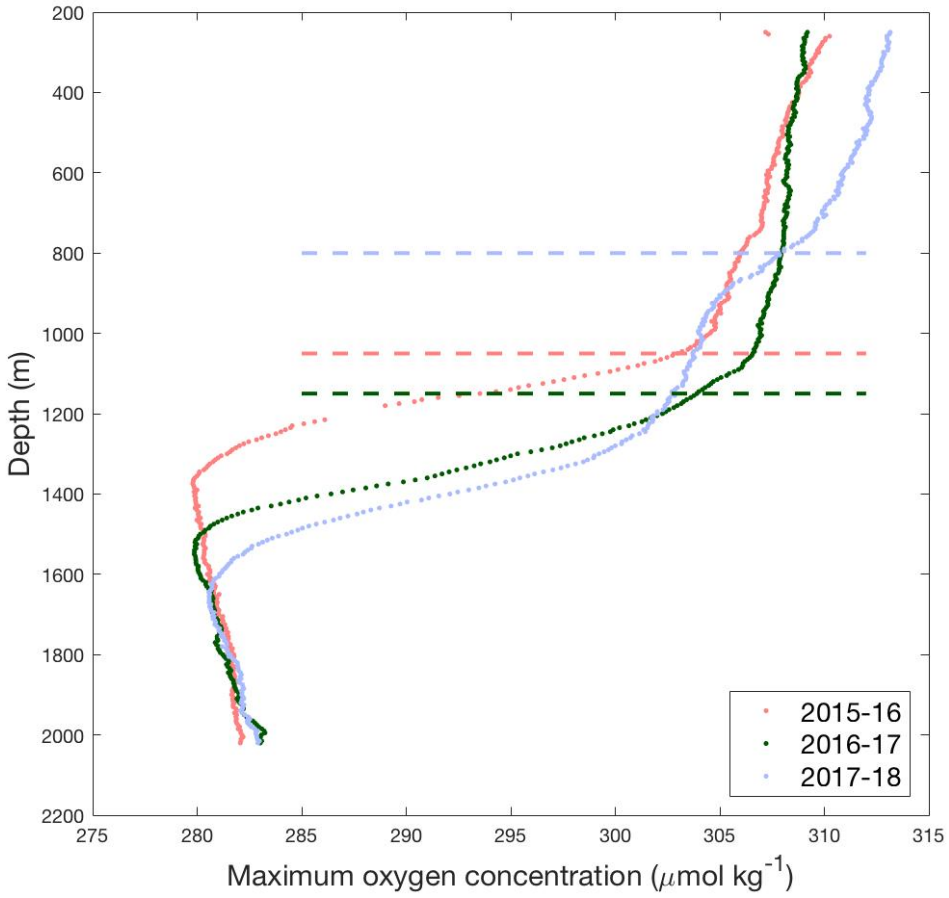

Figure 12. Depth profile of maximum oxygen concentrations at each depth for each year. Color-coded dotted lines indicate the winter ventilation depth for each year.

The three winter ventilation depths over the 2014-2018 period were much deeper than the average winter ventilation depths in the Irminger Sea over the last few decades. From 2003 to 2007, de Jong et al. (2012) found average winter ventilation depths that reached 400 meters. In 2008 and 2009, winter ventilation depths reached 800 and 1000 meters, respectively (de Jong et al., 2012). We see that the winter ventilation depths we found are particularly deep compared to the winter ventilation depths over the past two decades, which will ultimately affect the amount of carbon sequestered via the biological carbon pump.

3.3 Variation in annual respiration rates

Once the water column has re-stratified and the mixed layer has shoaled in the spring, the seasonally-ventilated thermocline -- below the shallow spring-summer mixed layer but above the winter ventilation depth -- is isolated from contact with the atmosphere. Oxygen concentrations then decrease over the course of the stratified season as sinking, dead phytoplankton and other organic matter are consumed and respired by heterotrophs in the thermocline. This respiration signature is evident in the water column as oxygen concentrations decrease over the course of the stratified season.

Figure 13 illustrates how dissolved oxygen patterns vary over time at two example depths in the water column. In Figure 13 A (500 m) we see that oxygen concentrations steadily increase during the mixing season, to a maximum oxygen concentration at the end of winter ventilation. Over the course of the stratified season, oxygen concentrations decrease to a minimum. The blue line illustrates the best fit line between the maximum and minimum oxygen concentrations, which is a proxy for respiration rate. We see this as a consistent pattern over all three stratified seasons, although the maximum and minimum oxygen values very annually. Figure 13 B (800 m) shows similar patterns, however, we see a smaller difference between maximum and minimum oxygen concentrations, which produces a shallower slope and a lower respiration rate. Higher respiration rates at 500 meters (Fig. 13 A) than 800 meters (Fig. 13 B) is consistent with the expected pattern of greater supply of organic matter available to be respired at shallower depths (Martin et al., 1987). Our goal is to quantitatively interpret these patterns to calculate respiration rates at each depth and total annual respiration.

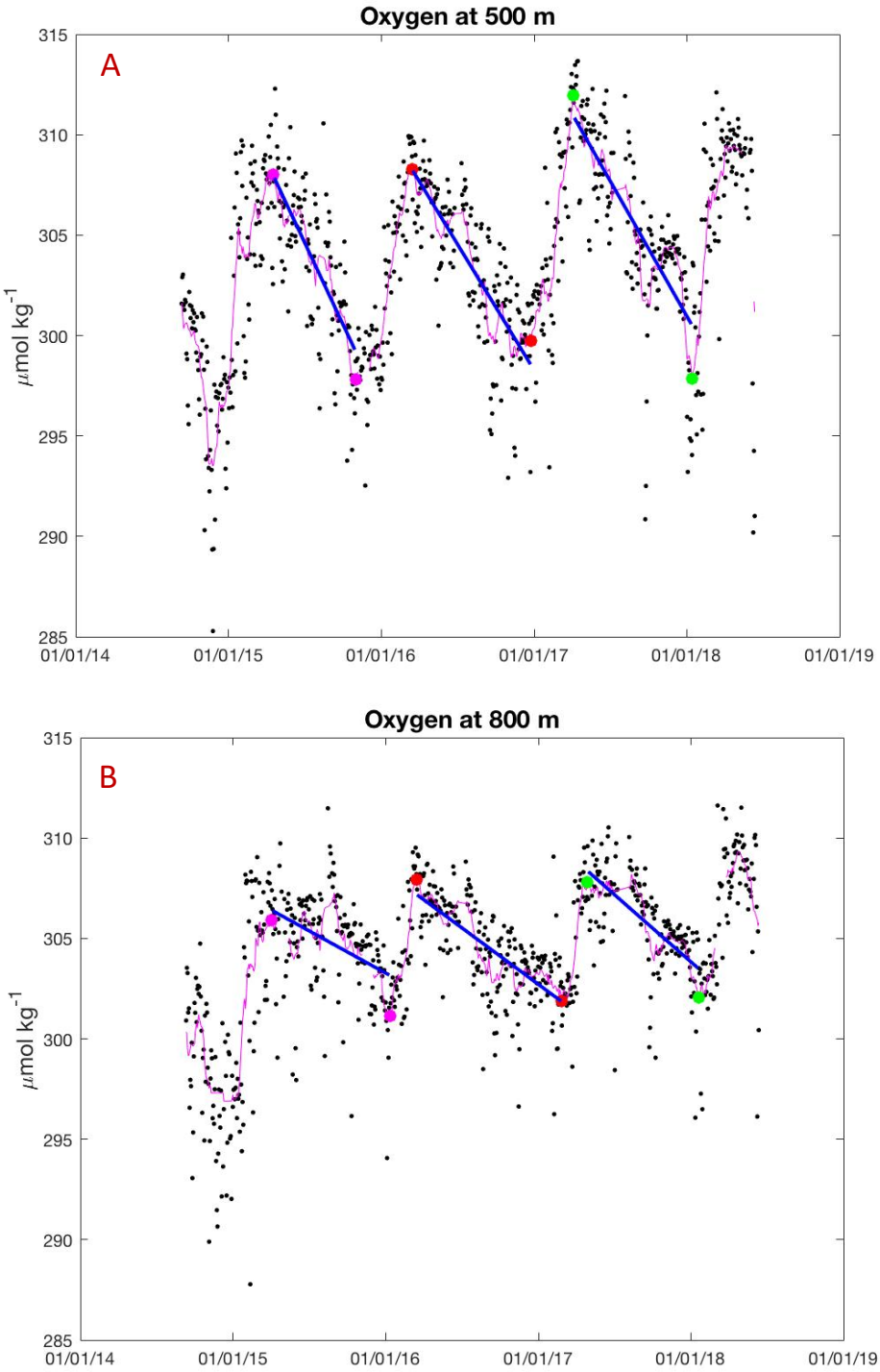

Figure 13. Dissolved oxygen time series at A) 500 meters and B) 800 meters. Black dots show the calibrated oxygen data without any smoothing. Pink lines show the smoothed data, determined by taking the moving mean across 15 sequential oxygen profiles. Pink, red, and green dots indicate the minimum and maximum oxygen concentrations for each stratified season. Blue lines illustrate a best fit line for the oxygen concentrations during the stratified season (between the dates of the maximum and minimum oxygen concentrations) of each year.

When calculating respiration rates, there are two factors that influence the total respiration over a stratified season. The first factor is the respiration rate per day at each depth, and the second is the length of the stratified season at each depth.

(Eq. 3) Total stratified season respiration = daily respiration rate * length of stratified season

In order to calculate annual respiration rates, we employ two methods. The first method involves subtracting the minimum oxygen value from the maximum oxygen value at each depth, then integrating through the entire water column to calculate a respiration rate. The second method involves fitting a line to the oxygen data to calculate the rate of oxygen change per day. The advantage of the second method is that individual oxygen data points will not skew the results, while the first method relies on only two oxygen data points at each depth to produce a respiration rate for that depth. In the second method, we fit a line to the data so at any one depth, the slope at that point depends on more than two data points. A downside of the linear fit method is that it assumes the respiration rate is constant over the course of the year, introducing a different type of uncertainty. Figure 14 compares the linear fit method across all three stratified seasons in order to visualize how respiration rates are similar or different annually. This figure does not account for depth dependent variation in length of the stratified season. Figure 16 accounts for the length of the stratified season at each depth and illustrates total annual respiration rates calculated using both methods.

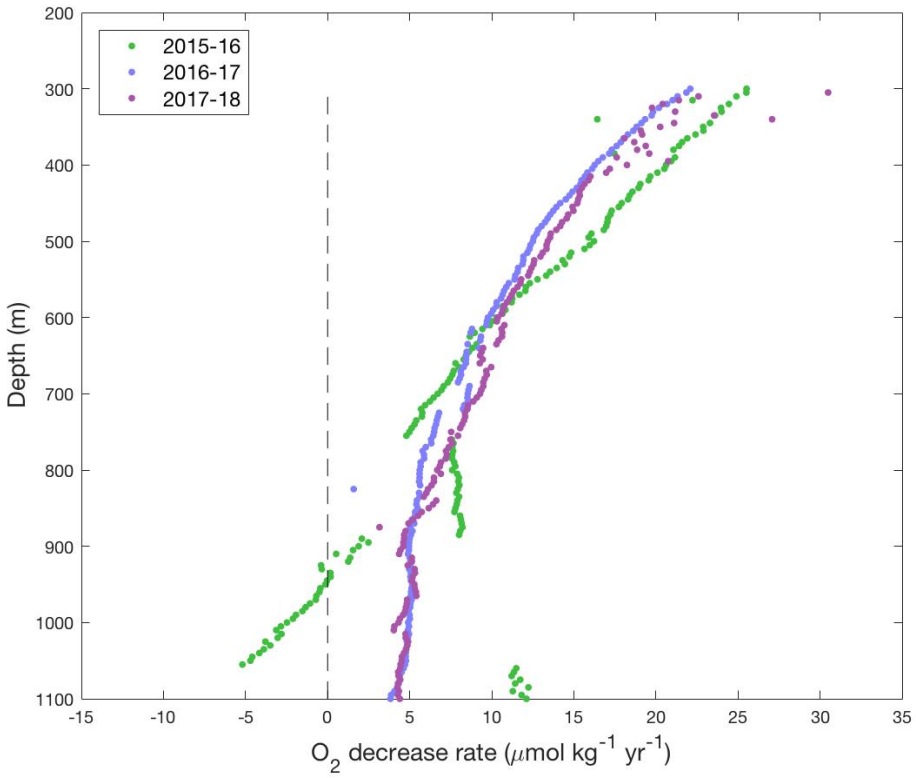

Figure 14. Annual respiration rates across the three years based on slope of linear fit over each stratified season. Daily respiration rates are multiplied by the length of a year to get an annual respiration rate. The length of the stratified season at each depth is not accounted for in this figure.

We calculated the length of the stratified season, defined as the time between the maximum and minimum oxygen values for each year, at 5-meter depth intervals. Deeper isotherms stratify sooner and mix later than shallower isotherms, so we expect the length of the stratified season to be longer in deeper isotherms. We find this to be true for 2015-16 and 2016-17, however we find that in 2017-18 the length of the stratified season at 400-500 meters is longer than at 700-800 meters (Table 3). This is likely due to uncertainty in the algorithm used to identify the beginning and end dates of stratification based on maximum and minimum oxygen values. We also find that the length of the stratified season for 2015-16 is much shorter at 400-500 meters than in other years because the minimum oxygen value was reached much earlier in this year than in 2016-17 or 2017-18 (Fig. 14).

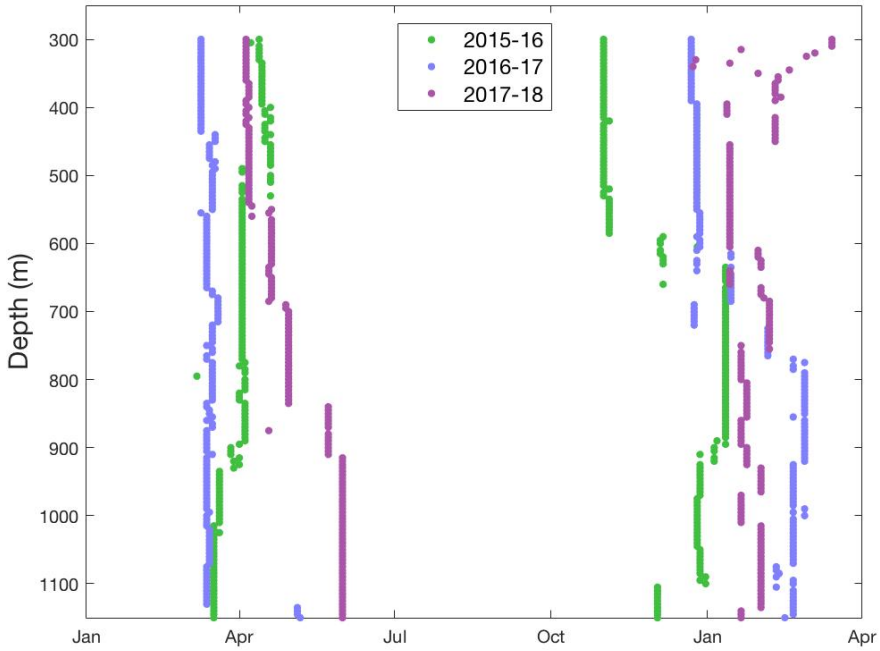

Figure 15. Beginning and end of the stratified season for all three years. Colors indicate the years of the stratified season. The beginning and end of the stratified season is marked by the maximum and minimum oxygen concentrations at each depth, respectively.

Table 3. Summary of the length (in days) for each stratified season, averaged across a range of depths.

Year	Average stratified season length from 400- 500 m	Average stratified season length from 700- 800 m	Average stratified season length from 900- 1000 m
Year 1 (2015-16)	198	285	280
Year 2 (2016-17)	287	322	347
Year 3 (2017-18)	292	274	N/A

Figure 16 shows higher total stratified season respiration rates closest to the sea surface and lower respiration rates at deeper depths. This pattern is consistent across all three years and in both methods. This is the pattern that we would expect as there is more biological activity closer to the sea surface, and therefore higher respiration rates (Martin et al., 1987). The duration of the stratified season varies with depth, affecting respiration rates. Generally, deeper depths stratify earlier and also ventilate later in the year than shallower depths, meaning there is a longer period of time across which respiration occurs (Fig. 14, Table 3). The

duration of the stratified season is a key parameter to consider, as it is one of the two variables used to calculate total respiration rates per year.

We see some unexpected deviations in the smoothed line during the 2015-16 season (Figure 16). However, since the greatest deviation in the line occurs at depths greater than 1,050 meters, these deviations will not be included in the respiration calculations, as we only integrate to 1,050 meters for the 2015-16 season.

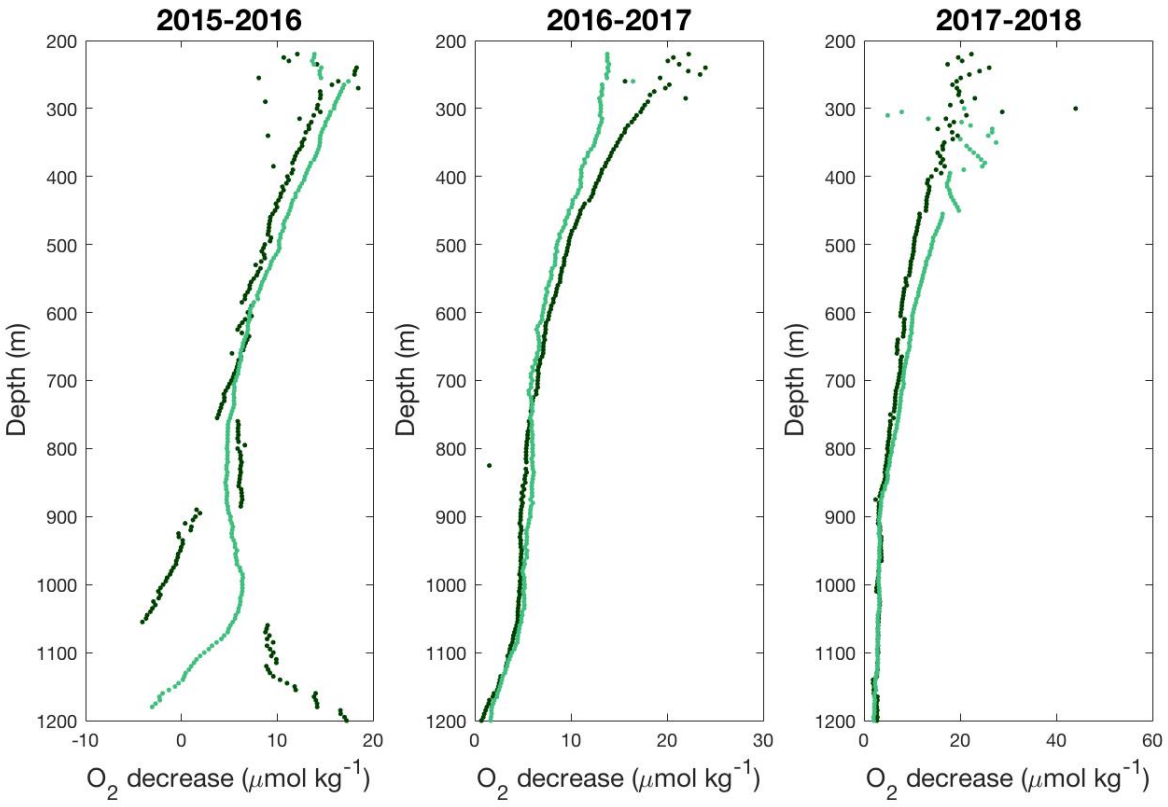

Figure 16. Two methods for calculating annual respiration rates for all three stratified seasons. Light green lines represent respiration rates calculated as the minimum oxygen value at the end of stratification subtracted from the maximum oxygen value at the end of winter ventilation. Dark green lines represent respiration rates calculated using a best fit linear method, representing the rate of oxygen change per day. Values were calculated every 5 meters in the water column.

After calculating respiration rates at five meter intervals, we integrated all respiration rates through the water column to calculate the total amount of respiration within the seasonal thermocline. Respiration rates for 2015-16 and 2016-17 were summed from 240 meters to the

depth of winter ventilation the following year. Data from 200 to 400 meters during the 2017-18 season were excluded due to a high number of missing data points that precluded accurate respiration calculations, so respiration rates were calculated from 400 meters to the depth of winter ventilation the following year. After calculating respiration rates in moles of oxygen, we converted moles of oxygen to moles of carbon in order to calculate the amount of carbon ventilated back into the atmosphere the following winter. Table 4 summarizes the respiration rates we calculated using both methods.

In order to understand if the lower total respiration rate calculated for the 2017-18 season (compared to 2015-16 and 2015-17) was due to integrating starting at 400 m, rather than 240 m, we calculated what the total respiration rate would have been for 2015-16 and 2016-17 if we had integrated starting at 400 m. For 2015-16, we calculated 4.4 mol O_2 m^{-2} using method 1 and 3.6 mol O_2 m^{-2} using method 2. For 2016-17, we calculated 4.8 mol O_2 m^{-2} using method 1 and 4.8 mol O_2 m^{-2} using method 2. These numbers are much closer to the values calculated for 2017-18, showing that the respiration rates at shallower depths are much higher than at deeper depths and therefore contribute more to the total thermocline respiration calculation.

We calculated the percent difference between the two methods for each year and found 18% difference in 2015-16, 12% difference in 2016-17, and 31% difference in 2017-18. Given that there is not a systematic difference between the two methods, I interpret the results by comparing both methods. The two methods produce slightly different respiration rates depending on the depth at which the rate is calculated. For example, in Figure 13 A, we see that during the 2016-17 season the total magnitude of the best fit line is greater than the total magnitude between the minimum and maximum oxygen concentrations calculated. Therefore, a greater respiration rate was calculated using a best fit line. Conversely, in the 2017-18 season, the magnitude of best fit line is smaller than the magnitude of the difference between the maximum and minimum oxygen values calculated, producing a larger respiration rate using the max-min method. Figure 16 also illustrates depth-specific respiration rates through the full water column.

Table 4. Respiration rates calculated using two methods. Method 1 involved subtracting minimum oxygen concentration from maximum oxygen concentrations at each depth. Method 2 involved using a best fit line to calculate the rate of oxygen change at each depth.

Respiration Rate	**2015-2016** *Integration range: 240 – 1050 m*	**2016-2017** *Integration range: 240 – 1150 m*	**2017-2018** *Integration range: 400 – 800 m*
Method 1 (mol O_2 m^{-2})	6.85	6.89	4.73
Method 2 (mol O_2 m^{-2})	5.83	7.66	3.62
Method 1 (mol C m^{-2})	4.89	4.92	3.38
Method 2 (mol C m^{-2})	4.16	5.47	2.59

When considering the components of the biological carbon pump, we consider the amount of organic matter produced at the sea surface, the amount that is respired while sinking through the water column, and the amount that sinks below the winter ventilation depth for long-term storage. Our data only accounted for the amount of carbon that was respired in the water column. We still do not have data that can accurately tell us how much total organic material was produced at the sea surface. However, our annual respiration rates are larger than the *total* amount of carbon that sank beneath the winter ventilation depth at open ocean time series sites (3 ± 1 mol C m^{-2} yr^{-1}), meaning that the total amount of organic material that is both respired in the thermocline and sinks below the winter ventilation depth is much larger in the Irminger Sea than at average open ocean sites (Emerson, 2014). This shows the crucial importance of accounting for how much carbon is respired and exchanged back into the atmosphere when calculating the total amount of carbon sequestered via the biological carbon pump.

3.4 Relationship between deep convection and respiration

We see that annual respiration rates are dependent on both the top depth of integration and the winter ventilation depth. Figure 16 shows similar respiration rates at each depth and across all years, so the main difference that leads to a smaller respiration rate in the 2017-18 stratified season is the top and bottom depth of integration. Integrating over 400 meters during the 2017-18 stratified season produced much lower respiration rates than integrating over ~800 meters during the 2015-16 and 2016-17 stratified seasons. This is mainly due to excluding the top portion of the thermocline where there are the highest respiration

rates. Differences in annual respiration rates across years could be attributed to differences in the amount of sinking organic matter respired at a given layer within the thermocline. However, because we see similar respiration rates at most depths across all years, we conclude that the top depth of integration and the variation in winter ventilation depths are the main factors influencing annual respiration rates. This shows that when quantifying how much carbon is sequestered annually, it is crucial to consider the winter ventilation depth in order to produce the most accurate estimate of how much carbon is ventilated back into the atmosphere.

3.5 Particulate organic carbon (POC) and chlorophyll

The respiration rates calculated above show that a large amount of organic carbon left the sea surface, was respired in the water column, and subsequently ventilated into the atmosphere the following winter. However, we still do not know how much organic carbon sank below the winter ventilation depth. Backscatter and chlorophyll are two types of data that will allow us to identify and quantify sinking particles sinking beneath the winter ventilation depth for long-term storage.

Both Chlorophyll and POC are tracers of organic matter in the water column. In the Irminger Sea, we see a huge phytoplankton bloom during the springtime months, corresponding with a large increase in surface chlorophyll concentrations. Measurements taken from the profiler mooring show that chlorophyll can also be seen at depth and can trace the deep mixing signature (Figure 17). We know that the chlorophyll measured at depth must be due to a physical, rather than biological, process, as phytoplankton do not grow at these depths. We also see the chlorophyll signature following the same pattern of deep mixing, with shallower isotherms mixing before deeper isotherms.

The POC measurements show sinking organic carbon particles within the water column. The patches of darker green seen in Figure 17 B are spikes in POC and are evidence of large sinking particles in the water column. These spikes are also evident in Figure 18 B where we see some measurements exceeding 0.001 m^{-1} which indicate large particles sinking throughout the water column. POC measurements shown in Figure 18 A will eventually be used to calibrate the backscatter data shown in Figure 18 B, and enable quantitative interpretation of the time-series

backscatter data from the profiler mooring to determine the total amount of POC sequestered below the winter ventilation depth.

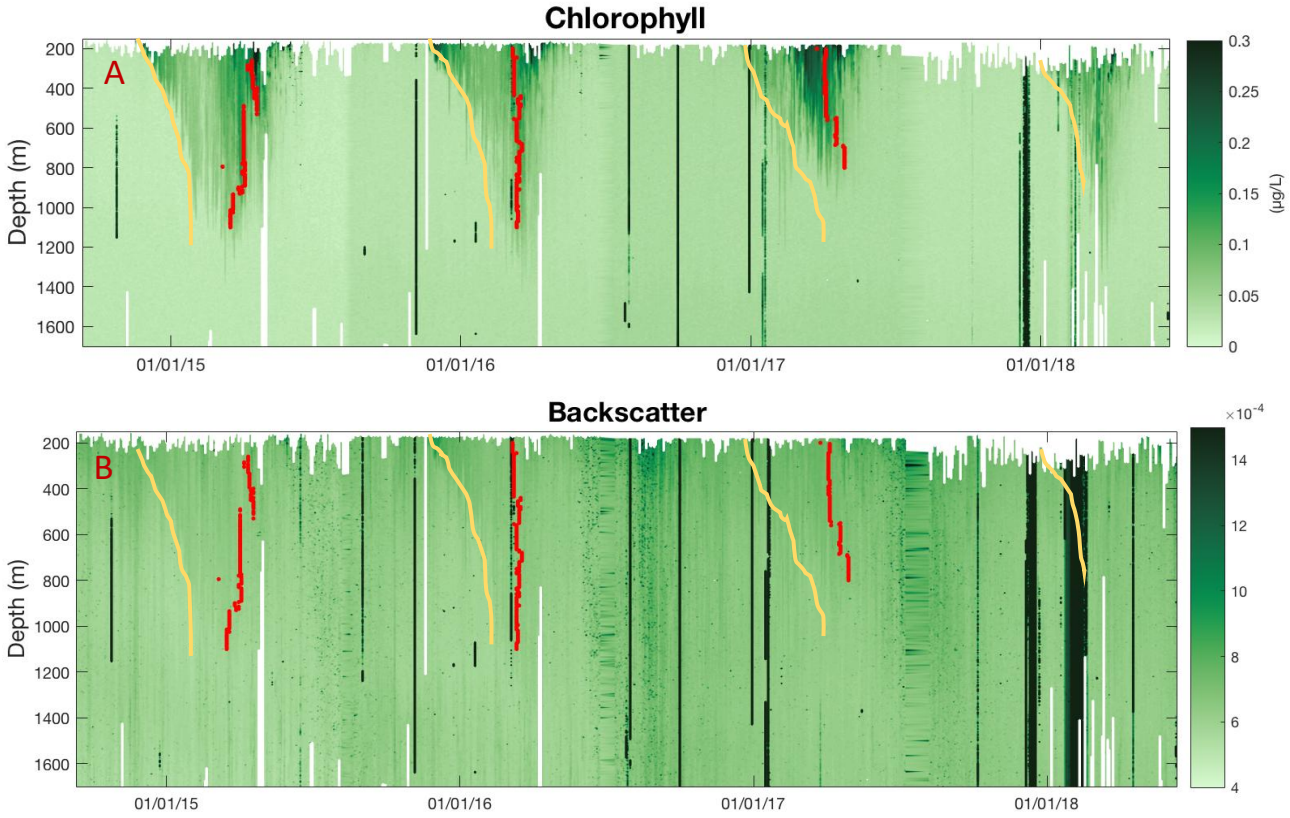

Figure 17. Time series of A) Chlorophyll and B) Backscatter from the profiler mooring over the four-year period. Yellow lines indicate the onset of ventilation and red lines indicate the end of ventilation, calculated as the maximum oxygen concentration at each depth.

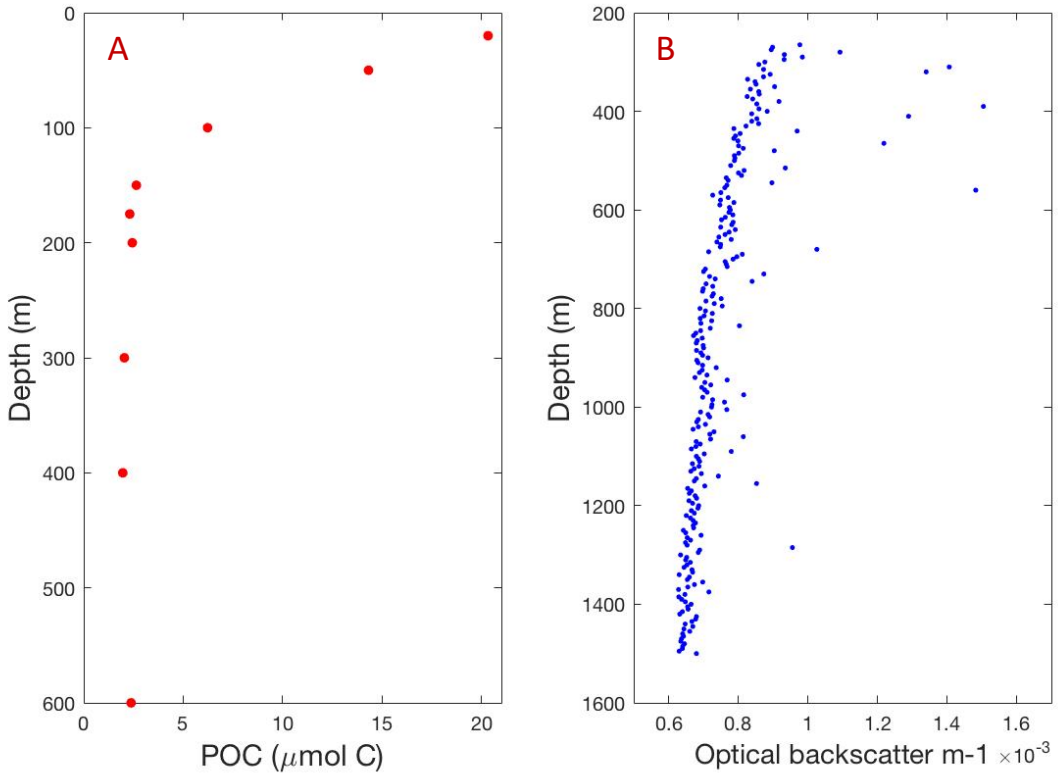

Figure 18. A) Depth profile of particulate organic carbon profile collected from cast 6 during the Irminger-005 cruise. Note that this CTD cast was performed in order to collect discrete data to calibrate the profiler mooring. B) Depth profile of optical backscatter which was collected by the profiler mooring within 1 day of the CTD cast that collected discrete samples to produce A. Note the different y-axes.

Conclusions and Future Work

Our analysis of spatial variation in winter ventilation depths across the Irminger Basin show that winter ventilation depths vary on the order of hundreds of meters throughout the basin. We found that all winter ventilation depths during the 2017-18 winter season reached at least 1,000 meters, much higher than the average winter ventilation depth over the past two decades (de Jong et al., 2012). Our calculations of both winter ventilation depths and respiration rates from the 2014-2018 time series of data collected by the profiler mooring in the Irminger Sea show strong interannual variability in both winter ventilation depths and respiration within the seasonally-ventilated thermocline, which determines the amount of carbon ventilated back to the atmosphere each winter. Winter ventilation depths range from 800 to 1,150 meters over the four-year time period, and depth-integrated respiration rates within the seasonally-ventilated thermocline range from 3.6 to 7.7 mol O_2 m^{-2}, corresponding to 5.5 to 2.6 mol C m^{-2} ventilated back into the atmosphere. We conclude that annual differences in total respiration depend on the portion of the water column ventilated each year. Depth-specific respiration rates do not seem to influence the total amount of carbon ventilated back into the atmosphere, whereas winter ventilation depth is a prominent factor in total respiration rates. We also see that the top portion of the water column (200 – 400 m), where respiration rates are highest, accounts for a large portion of the total carbon that is ventilated back into the atmosphere.

The next steps of this research include fully calibrating the chlorophyll and backscatter data in order to accurately quantify the amount of organic material sinking through the water column and penetrating below the winter ventilation depth. By using profiles made from discrete measurements taken while on research cruises, we will compare values from discrete samples with values collected by the profiler mooring. Using this calibrated data in conjuncture with dissolved oxygen data, we may precisely quantify not just how much carbon is exchanged back into the atmosphere, but how much sinks below the winter ventilation depth for long-term storage.

The results of my research have far-reaching implications for fulling understanding the role of the ocean in taking up carbon dioxide from the atmosphere. Over the 21st century, some

models predict a decline in the depth of deep convection, or a complete collapse in deep convection (Sgubin et al., 2017). In these scenarios, winter ventilation depths will be shallower, so interannual variability in deep mixing will be even more crucial to consider as respiration rates are higher at shallower depths, and therefore a slight change in winter ventilation depth would produce a larger change in the amount of carbon ventilated back into the atmosphere.

It is critical to better understand how high latitude places like the Irminger Sea take up carbon dioxide from the atmosphere, as the North Atlantic Ocean is a key driver in carbon sequestration, taking up anthropogenic carbon at three times the global rate (Sabine et al., 2004). When considering the role of the biological carbon pump in taking up carbon, we must also consider how physical processes, like deep mixing, affect the fate of that carbon in the long-term. We also see from our research and previous studies that the depth of winter mixing is highly variable, and in order to fully understand how areas of the ocean take up carbon, we account for interannual variations and better constrain these parameters using long-term data sets like the OOI array.

References:

Behrenfeld, M. J. (2010). Abandoning Sverdrup's Critical Depth Hypothesis on phytoplankton blooms. *Ecology*, *91*(4), 977–989.

Briggs, N., Perry, M. J., Cetinić, I., Lee, C., D'Asaro, E., Gray, A. M., & Rehm, E. (2011). High-resolution observations of aggregate flux during a sub-polar North Atlantic spring bloom. *Deep-Sea Research Part I: Oceanographic Research Papers*, *58*(10), 1031–1039.

Buckley, M. W., & Marshall, J. (2016). Observations, inferences, and mechanisms of the Atlantic Meridional Overturning Circulation: A review. *Reviews of Geophysics*, *54*(1), 5–63.

Chlorophyll Concentration (1 Month – AQUA/MODIS). (2015). Retrieved from https://neo.sci.gsfc.nasa.gov/

Ducklow, H. W., Steinberg, D. K., & Buesseler, K. O. (2001). Upper Ocean Carbon Export and the Biological Pump. *Oceanography*, *14*(4), 50–58.

Ehrhardt, M., & Koeve, W. (2007, December 27). Determination of particulate organic carbon and nitrogen. *Methods of Seawater Analysis*.

Fröb, F., Olsen, A., Våge, K., Moore, G. W. K., Yashayaev, I., Jeansson, E., & Rajasakaren, B. (2016). Irminger Sea deep convection injects oxygen and anthropogenic carbon to the ocean interior. *Nature Communications*, *7*, 13244.

Garcia, H. E., & Gordon, L. I. (1992). Oxygen solubility in seawater: Better fitting equations. *Limnology and Oceanography*, *37*(6), 1307–1312.

Hennon, T. D., Riser, S. C., & Mecking, S. (2016). Profiling float-based observations of net respiration beneath the mixed layer. *Global Biogeochemical Cycles*, *30*(6), 920–932.

Henson, S. A., Dunne, J. P., & Sarmiento, J. L. (2009). Decadal variability in North Atlantic phytoplankton blooms. *Journal of Geophysical Research: Oceans*, *114*(4), 1–11.

de Jong, M. F., Van Aken, H. M., Våge, K., & Pickart, R. S. (2012). Convective mixing in the central Irminger Sea: 2002-2010. *Deep-Sea Research Part I: Oceanographic Research Papers*, *63*, 36–51.

de Jong, D., Oltmanns, M., Karstensen, J., & Society, T. O. (2018). Deep convection in the Irminger Sea observed with a dense mooring array. *Oceanography*, *31*(1), 50–59.

de Jong, M. F., & de Steur, L. (2016). Strong winter cooling over the Irminger Sea in winter 2014–2015, exceptional deep convection, and the emergence of anomalously low SST. *Geophysical Research Letters*, *43*(13), 7106–7113.

Körtzinger, A., Send, U., Lampitt, R. S., Hartman, S., Wallace, D. W. R., Karstensen, J., et al. (2008). The seasonal pCO2 cycle at 49°N/16.5°W in the northeastern Atlantic Ocean and what it tells us about biological productivity. *Journal of Geophysical Research: Oceans*, *113*(4), 1–15.

Lamb, P. J., & Peppler, R. A. (1987). North Atlantic Oscillation: Concept and an Application. *Bulletin of the American Meteorological Society*, *68*(10), 1218–1225.

Laws, E. A. (1991). Photosynthetic quotients, new production and net community production in the open ocean. *Deep-Sea Research*, *38(1)*, 143–167.

Lozier, M. S. (2011). Overturning in the North Atlantic. *Annual Review of Marine Science*, *4*(1), 291–315.

Lozier, M. S., Li, F., Bacon, S., Bahr, F., Bower, A. S., Cunningham, S. A., et al. (2019). A sea change in our view of overturning in the subpolar North Atlantic. *Science*, *363*(6426), 516 LP-521.

Mahadevan, A., D'Asaro, E., Lee, C., & Perry, M. J. (2012). Eddy-driven stratification initiates North Atlantic spring phytoplankton blooms. *Science*, *336*(6090), 54–58.

Marshall, J., & Schott, F. (1999). Open-ocean convection: Observations, theory, and models. *Reviews of Geophysics*, *37*(1), 1–64.

Martin, J. H., Knauer, G. A., Karl, D. M., & Broenkow, W. W. (1987). VERTEX: carbon cycling in the northeast Pacific. *Deep Sea Research Part A. Oceanographic Research Papers*, *34*(2), 267–285.

Palevsky, H. I., & Nicholson, D. P. (2018). The North Atlantic Biological Pump: Insights from the Ocean Observatories Iniative Irminger Sea Array. *Oceanography*, *31*(1).

Pickart, R. S., Spall, M. A., Ribergaard, M. H., Moore, G. W. K., & Milliff, R. (2003). Deep convection in the Irminger sea forced by the Greeland trip jet. *Nature*, *424*, 152–156.

Piron, A., Thierry, V., Mercier, H., & Caniaux, G. (2016). Deep-Sea Research I Argo float observations of basin-scale deep convection in the Irminger sea during winter 2011 – 2012. *Deep-Sea Research Part I*, *109*, 76–90.

Sabine, Christopher L., Feely, Richard A., Gruber, Nicolas, Key, Robert M., Lee, K. (2004). The Oceanic Sink for Anthropogenic CO2. *Science*, *305*(5682), 367–371.

Sanders, R., Henson, S. A., Koski, M., De La Rocha, C. L., Painter, S. C., Poulton, A. J., et al. (2014). The Biological Carbon Pump in the North Atlantic. *Progress in Oceanography*, *129*(PB), 200–218.

Sgubin, G., Swingedouw, D., Drijfhout, S., Mary, Y., & Bennabi, A. (2017). Abrupt cooling over the North Atlantic in modern climate models. *Nature Communications*, *8*, 14375.

Sverdrup, H. U. (1953). On conditions for the vernal blooming of phytoplankton. *Journal of Marine Science*, *18*(3), 287–295.

Takeshita, Y., Martz, T. R., Johnson, K. S., Plant, J. N., Gilbert, D., Riser, S. C., et al. (2013). A climatology-based quality control procedure for profiling float oxygen data. *Journal of Geophysical Research: Oceans*, *118*(10), 5640–5650.

The Keeling Curve. (2019). Retrieved from https://scripps.ucsd.edu/programs/keelingcurve/

Våge, K., Pickart, R. S., Moore, G. W. K., & Ribergaard, M. H. (2008). Winter Mixed Layer Development in the Central Irminger Sea: The Effect of Strong, Intermittent Wind Events. *Journal of Physical Oceanography*, *38*(3), 541–565.

Våge, K., Pickart, R. S., Thierry, V., Reverdin, G., Lee, C. M., Petrie, B., et al. (2008). Surprising return of deep convection to the subpolar North Atlantic Ocean in winter 2007–2008. *Nature Geoscience*, *2*, 67.

Westberry, T. K., Schultz, P., Behrenfeld, M. J., Dunne, J. P., Hiscock, M. R., Maritorena, S., et al. (2016). Annual cycles of phytoplankton biomass in the subarctic Atlantic and Pacific Ocean. *Global Biogeochemical Cycles*, *30*(2), 175–190. https://doi.org/10.1002/2015GB005276

Wolf, M. K., Hamme, R. C., Gilbert, D., Yashayaev, I., & Thierry, V. (2018). Oxygen saturation surrounding deep-water formation events in the Labrador Sea from Argo-O2 data. *Global Biogeochemical Cycles*.